RESEARCH ARTICLE

Hubs of long-distance co-alteration characterize brain pathology

Franco Cauda[1,2] | Lorenzo Mancuso[1,2] | Andrea Nani[1,2] | Linda Ficco[1,2] | Enrico Premi[3,4] | Jordi Manuello[1,2] | Donato Liloia[1,2] | Gabriele Gelmini[2] | Sergio Duca[1] | Tommaso Costa[1,2]

[1]GCS-fMRI, Koelliker Hospital and Department of Psychology, University of Turin, Turin, Italy

[2]FOCUS Lab, Department of Psychology, University of Turin, Turin, Italy

[3]Stroke Unit, Azienda Socio-Sanitaria Territoriale Spedali Civili, Spedali Civili Hospital, Brescia, Italy

[4]Centre for Neurodegenerative Disorders, Neurology Unit, Department of Clinical and Experimental Sciences, University of Brescia, Brescia, Italy

Correspondence
Franco Cauda, FocusLab and GCS fMRI, Koelliker Hospital and Department of Psychology, University of Turin, Turin, Italy.
Email: franco.cauda@unito.it

Funding information
Fondazione Sanpaolo, Turin

Abstract

It is becoming clearer that the impact of brain diseases is more convincingly represented in terms of co-alterations rather than in terms of localization of alterations. In this context, areas characterized by a long mean distance of co-alteration may be considered as hubs with a crucial role in the pathology. We calculated meta-analytic transdiagnostic networks of co-alteration for the gray matter decreases and increases, and we evaluated the mean Euclidean, fiber-length, and topological distance of its nodes. We also examined the proportion of co-alterations between canonical networks, and the transdiagnostic variance of the Euclidean distance. Furthermore, disease-specific analyses were conducted on schizophrenia and Alzheimer's disease. The anterodorsal prefrontal cortices appeared to be a transdiagnostic hub of long-distance co-alterations. Also, the disease-specific analyses showed that long-distance co-alterations are more able than classic meta-analyses to identify areas involved in pathology and symptomatology. Moreover, the distance maps were correlated with the normative connectivity. Our findings substantiate the network degeneration hypothesis in brain pathology. At the same time, they suggest that the concept of co-alteration might be a useful tool for clinical neuroscience.

KEYWORDS
Alzheimer's disease, network degeneration, pathology spread, physical distance, schizophrenia, topological distance, transdiagnostic, VBM

1 | INTRODUCTION

Converging evidence is revealing that the impact of diseases on brain structure is better appreciated not as the simple spatial distribution of lesions but as a system of interrelated alterations affecting networks (Evans, 2013). This likely happens in neurodegenerative diseases, where misfolded proteins frequently spread from one area to another in a prion-like fashion (Goedert, Masuda-Suzukake, & Falcon, 2017; Guest et al., 2011). This mechanism has been put forward to explain the development of anatomical alterations observed in such diseases in terms of connectivity pathways, along which pathological proteins (proteinopathy) or other toxic agents can propagate

Franco Cauda and Lorenzo Mancuso should be considered joint first authors.

(Mandelli et al., 2016; Manuello et al., 2018; Saxena & Caroni, 2011; Seeley, Crawford, Zhou, Miller, & Greicius, 2009; Warren et al., 2013; Warren, Rohrer, & Hardy, 2012). However, the network-like account of co-alterations seems to provide insights also in clinical conditions that do not have a neurodegenerative origin, such as schizophrenia, autism, obsessive-compulsive disorder, depression, and chronic pain (Cauda et al., 2014; Cauda et al., 2017; Cauda et al., 2018; Shafiei et al., 2019; Tatu et al., 2018; Wheeler et al., 2015; Wheeler et al., 2017). Furthermore, transdiagnostic meta-analyses merging data of studies about psychiatric and neurologic diseases support the following ideas: (a) the most affected areas of the brain correspond to the hubs of the functional and structural connectomes (Crossley et al., 2014), and (b) the distribution and development of co-alterations are mainly explained by functional and structural connectivity constraints (Cauda et al., 2018). Therefore, the anatomical substrate of brain disorders might be better accounted for by patterns of *co-alterations* than by the simple localization of a series of unrelated alterations.

A relevant feature of brain organization is the physical distance between interconnected areas. The small-world networks of the human connectome are composed by several clusters of short-range connectivity, linked together by long-range connections (Achard et al., 2006; Sporns & Zwi, 2004; Watts, Strogatz, & Tseng, 1998). Within an evolutionary perspective, the brain evolved to match a trade-off between minimizing wiring cost and allowing a fast, efficient, and resilient information flow (Bullmore & Sporns, 2012; Laughlin & Sejnowski, 2003). Nodes of long-range connectivity are to be considered central hubs of the connectome, as they tend to be connected with many other nodes, which makes them crucial in the interplay between segregation and integration that shapes brain structure and function (Alexander-Bloch et al., 2013; Bullmore & Sporns, 2012; Liao et al., 2013). As brain hubs with high centrality are also the regions more likely to be affected by pathology (Crossley et al., 2014), this organization is likely to be related to the distribution patterns of neuropathological alterations. Interestingly, both functional (Alexander-Bloch et al., 2013; Guo et al., 2014) and anatomical covariance networks (Bassett et al., 2008) of certain diseases, such as schizophrenia, have been associated with altered values of physical distance. Higher order associative brain regions, which are more prone to be damaged by diseases (Crossley et al., 2014), are characterized by a long physical distance and a high centrality (Sepulcre et al., 2010). So, if connectivity influences the development of pathology (Cauda, Nani, Manuello, et al., 2018; He, Chen, & Evans, 2007; Mandelli et al., 2016; Seeley et al., 2009; Zhou, Gennatas, Kramer, Miller, & Seeley, 2012), the spatial distribution of the physical distance of co-alterations might provide an insightful indication of how pathology is distributed across the brain. It would also be interesting to compare such information with a measure of centrality from a normative connectome, to test whether there is a correlation between abnormal distance and connectivity. This would help to clarify the relationship between co-alteration and connectivity, as well as to better understand the complex systems of alterations of the diseases brain. Finding a relation between co-alteration distance and connectivity would also be a further confirmation that pathology is bonded to normal connectivity (Cauda et al., 2019). In fact, since hubs facilitate dynamics of spread

across the brain (Mišić et al., 2015), it is more likely that long-range co-alterations and connectivity overlap in these regions. Thus, observing such overlap would emphasize the importance of brain hubs in the context of pathology, showing that they are not just the most damaged regions (Crossley et al., 2014), but also that they are involved in a long-range coupling of alterations.

Therefore, in the present study, we assessed the mean physical distance of co-alterations and its relationship with functional degree centrality (DC) in a meta-analytic, transdiagnostic way, so as to identify the cerebral areas that are more involved in long-range systems of pathological modifications. By searching in the BrainMap database, we retrieved both voxel-based morphometry (VBM) and activation data to be used in a meta-analytic technique based on the Patel's κ (Cauda, Nani, Costa, et al., 2018; Mancuso et al., 2019; Patel, Bowman, & Rilling, 2006). The κ is a Bayesian index proposed by Patel et al. (2006) to calculate functional connectivity with activation data obtained through a behavioral task. Previous publications of our group showed that it could also be used in a meta-analytic fashion, both on activation and alteration data (Cauda, Nani, Costa, et al., 2018; Mancuso et al., 2019; Manuello et al., 2018). The transdiagnostic approach was motivated by the assumption that the mechanisms underlying the phenomenon of co-alteration seem to be related to normative brain connectivity (Buckholtz & Meyer-Lindenberg, 2012; Cauda, Nani, Costa, et al., 2018). This relation could be, at least in part, explained by models of spread, as it seems to be in the case of neurodegenerative diseases (Raj & Powell, 2018). However, the concordance between the distribution of pathology and connectivity might be better understood as a multifactorial phenomenon, involving genetics, excitotoxicity, and trophic mechanisms too (Cauda et al., 2019). Regardless of the mechanisms involved, we might expect any relation or influence of connectivity on pathology to have a mostly disease-nonspecific effect.

We therefore constructed two transdiagnostic networks of co-alterations of gray matter (GM) decreases or increases comprising all the neurological and psychiatric diseases of the BrainMap database. On such networks, we calculated the mean Euclidean, fiber-length, and topological distances for each brain region. Then, we compared these distance maps with a map of meta-analytic DC of co-activations, so as to see whether the most connected areas of the functional healthy brain are also those with the longest co-alterations. Co-activations are known to reflect resting-state functional connectivity (Cauda et al., 2012; Eickhoff et al., 2010; Laird et al., 2009; Laird et al., 2013; Torta, Costa, Duca, Fox, & Cauda, 2013), thus this map of co-activation hubness could be taken as a proxy of functional DC. One advantage of using such meta-analytic map is that it has been produced with a similar method to that of mean distance of co-alteration, thus they can be compared more easily. Furthermore, mean Euclidean distance of co-activation, structural fiber-length, and topological distance maps were also produced and compared to those of co-activation.

These analyses were motivated by the general hypothesis that co-alterations are related, and possibly influenced, by normal connectivity (Cauda et al., 2019). Thereby, we expected that the regional mean of different forms of distance would correlate positively with the measures of co-activation. Of the various distances, the Euclidean

distance was the one we expected the most to show a good fit with the co-activation maps, because of the aforementioned biological relevance of the physical separation between brain regions. In fact, close regions are more likely to be connected than distant ones (Bellec et al., 2006; Salvador et al., 2005). The fiber-length and topological distances were taken to model more accurately the spread dynamics compared to the Euclidean distance that seems to be less theoretically characterized than the others. More in detail, as the topological distance would express an epidemic model of contagion, we were interested in comparing it to the fiber-length, which would represent the distance traveled by a toxic agent along the axon. We speculated that more general models would fit better the normative connectivity (i.e., Euclidean > topological > fiber length) because they would better represent the multifactorial nature of pathoconnectivity.

Moreover, since we believed the transdiagnostic approach would prevent us from drawing any conclusion about the specific disease, first we investigated the transdiagnostic variability of each voxel and network. Finally, taking schizophrenia and Alzheimer's disease as representative examples of a single-pathology approach for psychiatric and neurologic diseases, we calculated their maps of mean Euclidean distance of co-alterations. These analyses showed that the anatomical distribution of the mean distance can provide an insightful index of the pathologic spread of single diseases.

2 | MATERIALS AND METHODS

2.1 | Collection of data

In the present study, the Cochrane Collaboration definition of meta-analysis (Green et al., 2008) was adopted and the selection of articles was conducted referring to the "PRISMA statement" international guidelines (Liberati et al., 2009; Moher, Liberati, Tetzlaff, & Altman, 2009). See Figure 1 for the PRISMA flow chart. Neuroimaging experiments eligible for the analysis were retrieved from BrainMap (http://brainmap.org/) (Fox et al., 2005; Fox & Lancaster, 2002; Laird, Lancaster, & Fox, 2005; Vanasse et al., 2018). BrainMap is an open access online database constituted by over 15,000 neuroimaging experiments and 120,000 locations in stereotaxic brain space. The database has two sections for VBM and functional data sets.

The VBM BrainMap section was queried (December 2019) with the following algorithms:

1. [Experiments Context is Disease] AND [Experiment Contrast is Gray Matter] AND [Experiments Observed Changes is Controls>Patients];

2. [Experiments Context is Disease] AND [Experiment Contrast is Gray Matter] AND [Experiments Observed Changes is Patients>Controls].

The first step consisted in the codification of the VBM data set following the ICD-10 classification (World Health Organisation, 1992). Subsequently, full-text articles were analyzed in order to verify that they conformed with the following criteria: (a) being an original work

published in a peer-reviewed English language journal; (b) performing a whole-brain VBM analysis technique; (c) including a matched comparison between a pathological group and a group of healthy subjects; (d) reporting GM decrease/increase changes in the pathological sample; (e) adopting a specified VBM analysis; (f) referring to a specific stereotaxic space (e.g., Montreal Neurological Institute space or Talairach/Tournoux atlas) as regards GM increase/decrease changes. Basing on these criteria, we deemed eligible 1,001 experiments for GM decreases and 382 for GM increases. Descriptive information of interest was extracted from each full-text article fulfilling the abovementioned criteria. As a further specification, all the experiments not coded with F (i.e., mental, behavioral and neurodevelopmental disorders) or G (i.e., diseases of the nervous system) labels were excluded from the analysis. Moreover, studies related to codes that could not be considered as primary brain disorders (i.e., F10: alcohol-related disorders; F15: other stimulant-related disorders; F28: other psychotic disorders not due to a substance or known physiological condition; F91: conduct disorders; G11: hereditary ataxia; G43: migraine; G44: other headache syndromes; G47: sleep disorders; G50: disorders of trigeminal nerve; and G71: primary disorders of muscles) were also excluded. Articles including less than eight subjects were excluded as well. This lower bound was chosen in accordance with the work of Scarpazza, Tognin, Frisciata, Sartori, and Mechelli (2015), who demonstrated that VBM experiments based on an equivalent sample should not be biased by an increased false-positive rate. At the end of the selection procedure, 642 remaining experiments for the GM decreases (for 15,820 subjects and 7,704 foci) and 204 remaining experiments for the GM increases (for 4,966 subjects and 2,244 foci) were included in the analyses. We also calculated single-disease co-alteration networks using only on the data of schizophrenia and Alzheimer's disease (see Table S5). Furthermore, for those two diseases, we produced the anatomical likelihood estimation (ALE) (Eickhoff et al., 2009; Eickhoff, Bzdok, Laird, Kurth, & Fox, 2012; Laird et al., 2005a; Turkeltaub et al., 2012) maps of the VBM decreases and increases to be compared to the corresponding distance maps. The maps were thresholded at $p = .05$, with an FWE correction for multiple comparison as indicated by Eickhoff et al. (2016), and a cluster volume threshold of 100 mm. We chose these relatively lenient thresholds to ensure that any difference between the ALE and the co-alteration maps could not be imputed to an excessively rigorous ALE thresholding.

For the functional co-activation map, a systematic search was conducted through the entire functional data set of BrainMap with the following query:

[Experiments Context is Normal Mapping] AND [Experiments Activation is Activations Only] AND [Subjects Diagnosis is Normals].

This search produced 2,376 articles, for a total of 13,148 experiments, 112 paradigm classes, and 68,152 subjects (see Figure S1 for the PRISMA flowchart and Table S6). This data set represents the activations of normal subjects across all the functional paradigms of the BrainMap database. Finally, we converted all locations reported in MNI into Talairach space using the Lancaster's icbm2tal transform (Lancaster et al., 2007).
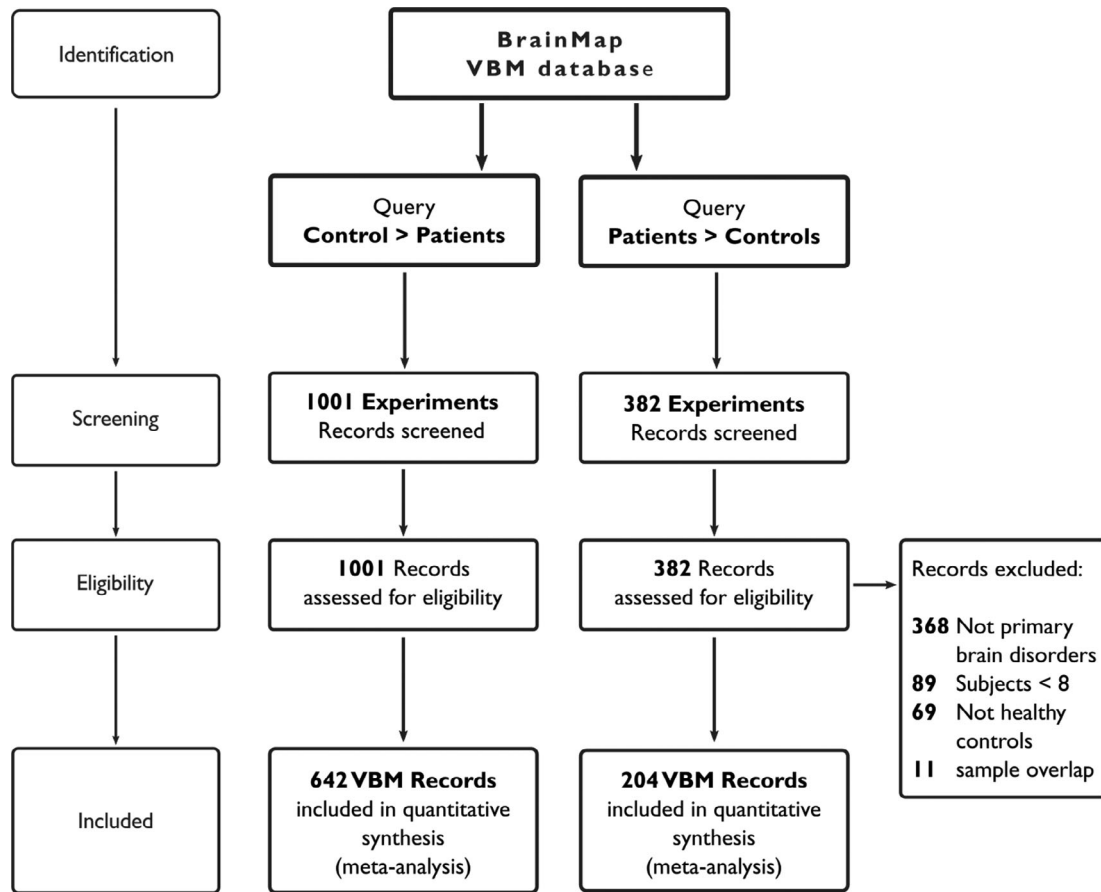
FIGURE 1 PRISMA flowchart of the selection of studies

2.2 | Modeled alteration maps

To obtain the alteration maps from the BrainMap foci, we adopted the ALE framework (Eickhoff et al., 2009; Eickhoff et al., 2012; Turkeltaub et al., 2012) to produce a modeled alteration (MA) map for each experiment (Figure 2a). To build the MA maps, every focus of each experiment is taken as the central point of a three-dimensional Gaussian distribution of probability:

$$p(d) = \frac{\exp\left(\frac{-d^2}{2\sigma^2}\right)}{\sigma^3 \sqrt{(2\pi)^3}}$$

In this formula d represents the Euclidean distance between the voxels and each considered focus, while the standard deviation σ represents the spatial uncertainty. The standard deviation is obtained through the full-width half-maximum (FWHM) and is defined as follows:

$$\sigma = \frac{\text{FWHM}}{\sqrt{8\ln 2}}$$

The FWHM is calculated as proposed by Eickhoff et al. (2009):

$$\text{FWHM} = \sqrt{U_{\text{temp}}^2 + \left(\frac{U_{\text{subj}}}{\sqrt{N_{\text{subjects}}}}\right)^2}$$

where U_{temp} and U_{subj} are the estimates of the between-subjects and between-templates variance. This calculation is done automatically using the GingerALE software.

2.3 | Co-alteration matrix calculation

The brain was partitioned on the basis of an anatomical atlas derived from the Talairach Daemon atlas with a resolution of 2 mm (Lancaster et al., 2000), a co-alteration matrix resulted from all the possible couples of brain areas. In the resulting ExR matrix, each of E row stands for an experiment, while each of R column reports a region; in the present study, the matrix included 642 experiments (VBM contrasts) × 1105 regions for the decrease condition, and 204 experiments × 1105 regions for the increase condition. For each experiment, a given brain region was considered altered if the experiment MA map showed 20% or more of significant voxels within the region (Figure 2b). The choice of this threshold is arbitrary, but it has already been proven that it does not affect the results significantly (Mancuso et al., 2019) and thus the use of
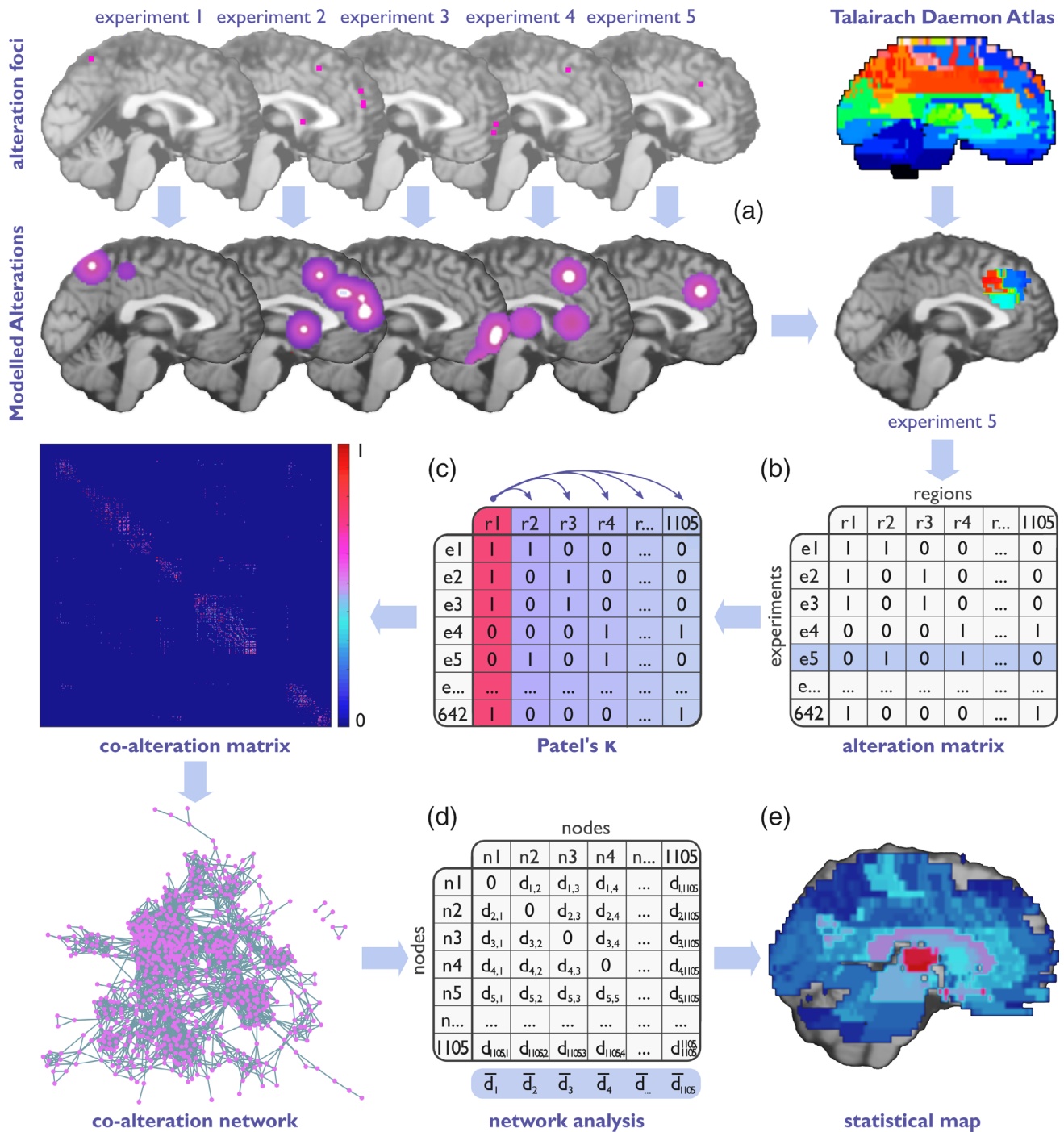
FIGURE 2 Illustration of the methods. (a) For each experiment included in a given meta-analysis (decreases or increases), a modeled alteration (MA; or activation) map is created placing a Gaussian distribution of probability around each reported focus of alteration (or activation). (b) For each experiment, each region of the atlas is considered to be altered if the 20% of its voxels is covered by the MA corresponding to that experiment. Thus, for each experiment, we obtain a vector of dichotomous values that represent the status of every region. (c) The Patel's κ is calculated between each one of such vectors and all the others, obtaining a network of co-alterations (or co-activations). Here, the co-alteration matrix and the network of the voxel-based morphometry decreases are shown. (d) Any network analysis can be computed on the resulting matrix. For instance, a measure of distance can be associated to each edge $x_{i,j}$ to calculate the mean distance of each node. Otherwise, a centrality measure such as the degree can be derived. (e) A statistical map can be produced assigning to the volumes of the atlas the values calculated for each node

different thresholds was not implemented in the present study. The use of Patel's κ index (Patel et al., 2006) allowed us to evaluate the probability of co-alteration of each couple of regions (Figure 2c). Given two regions (a and b), we can determine all their conjoint states of alteration

as follows: (a) a and b are both altered; (b) a is altered and b is not; (c) b is altered and a is not; (d) neither a nor b are altered. Thus, frequencies of these four cases recurring in all the experiments could be described by the following probability formulas:

$$\vartheta_1 = P(a = 1, b = 1)$$

$$\vartheta_2 = P(a = 1, b = 0)$$

$$\vartheta_3 = P(a = 0, b = 1)$$

$$\vartheta_4 = P(a = 0, b = 0)$$

These probabilities stand for the conjoint state frequencies of a couple of nodes (a and b) in the four possible combinations. Table 1 contains the marginal probabilities. Obtaining these probabilities allowed us to use the Patel's κ index to create the correlation matrix including each couple of brain areas. Patel's κ informs about the probability that two nodes are co-altered in opposition to the probability that they are altered independently on each other. Patel's κ is defined as follows:

$$\kappa = \frac{(\vartheta_1 - E)}{D(\max(\vartheta_1) - E) + (1 - D)}$$

where

$$E = (\vartheta_1 + \vartheta_2)(\vartheta_1 + \vartheta_3)$$

$$\max(\vartheta_1) = \min(\vartheta_1 + \vartheta_2, \vartheta_1 + \vartheta_3)$$

$$\min(\vartheta_1) = \max(0, 2\vartheta_1 + \vartheta_2 + \vartheta_3 - 1)$$

$$D = \begin{cases} \dfrac{\vartheta_1 - E}{2(\max(\vartheta_1) - E)} + 0.5, & \text{if } \vartheta_1 \geq E \\ 0.5 - \dfrac{\vartheta_1 - E}{2(E - \min(\vartheta_1))}, & \text{otherwise} \end{cases}$$

The numerator of the fraction is the difference between the likelihood that a and b are altered together and their expected joint alteration in a condition of independence, and the denominator is a weighted normalizing constant. $\max(\vartheta_1)$ represents the maximum value of conjoint probability $p(a, b)$, given $p(a)$ and $p(b)$, whereas $\min(\vartheta_1)$ represents the minimum value of $p(a, b)$, given $p(a)$ and $p(b)$. Patel's κ index returns values ranging from –1 and 1. A value of $|\kappa|$ that is close to one characterizes a high co-alteration. The statistical significance of Patel's κ is assessed by means of a simulation of a generative model of data based on the Monte Carlo's algorithm. Specifically, the algorithm computes an estimate of $p(\kappa|z)$ by sampling a Dirichlet distribution and

TABLE 1 Marginal probabilities between altered and unaltered regions

Region b	Region a		
	Altered	Unaltered	
Altered	ϑ_1	ϑ_3	$\vartheta_1 + \vartheta_3$
Unaltered	ϑ_2	ϑ_4	$\vartheta_2 + \vartheta_4$
	$\vartheta_1 + \vartheta_2$	$\vartheta_3 + \vartheta_4$	1

determining the proportion of the samples in which $\kappa > e$. The resulting co-alteration matrix returns values that are proportional to the statistical relationship between the patterns of brain areas' alterations taken into account.

2.4 | Co-activation matrix

The co-activation map was obtained applying the same method for the construction of the co-alteration matrix (i.e., Patel's κ index calculated on each couple of brain areas) to the BrainMap functional database of activations of healthy subjects.

2.5 | Measurement of the mean distances and calculation of the meta-analytic DC

For each significant statistical association between two regions a and b in the co-alteration (or co-activation) matrix, we calculated the respective Euclidean distance between the centroids of a and b in the Talairach Daemon atlas (Figure 2d). The fiber-length and topological distances were calculated on the HCP-842 DTI template released by Yeh and colleagues (Yeh et al., 2018), which is based on 842 subjects (age 22–35 years, M: 372 F: 470) of the 900 subject release of the Human Connectome Project (Van Essen et al., 2013). The fiber-length distance of each couple of areas was obtained with DSI studio (Yeh, Badre, & Verstynen, 2016; Yeh, Liu, Hitchens, & Wu, 2017; Yeh, Verstynen, Wang, Fernández-Miranda, & Tseng, 2013). Similarly, DSI Studio was also used to obtain the matrix of structural connectivity. After its binarization (which also included to set to zero all the edges that were nonsignificant in the corresponding co-alteration map), such matrix was used to calculate the shortest path between each couple of nodes through the Brain Connectivity Toolbox algorithms (Rubinov & Sporns, 2010). Then, for each form of distance, the mean distance of the significant connections of each node was assigned to the corresponding region of the atlas to obtain a map (Figure 2e).

To calculate the DC of co-activation, we employed the Brain Connectivity Toolbox algorithms (Rubinov & Sporns, 2010). Specifically, DC is defined as the number of edges incident upon a node. Since the κ calculation already performed a statistical thresholding, the binarization of the matrix consisted in setting all the nonzero values to one, and to calculate the DC as the sum of each column. Furthermore, to obtain the structural control maps of fiber-length and topological distance, the mean regional values of such distances were calculated as above, except that the edges that were nonsignificant in the κ matrix were not removed.

2.6 | Comparison between maps

In order to evaluate the similarity between the distance of the co-alteration map and the functional DC map, the correlation between these maps was calculated. To establish the involvement of each brain area to the correlation between the two maps, we applied the voxels'

contribution to correlation (VCC) technique (Mancuso et al., 2019). This *leave-one-out* procedure recursively computes the correlation between each couple of maps, subtracting one voxel at every run (the same voxel for both the maps). To create a map showing the contribution of each voxel to the correlation, the difference between the correlation value calculated in the whole maps and the correlation value obtained after the exclusion of each couple of voxels is associated to the singular voxel. Therefore, it is possible to visualize the extent to which the correlation value decreases or increases depending on the subtraction of each couple of corresponding voxels from the calculation. The normalized version of this map (transformed in order to range from –1 to 1) represents the stability of correlation and describes the contribution of each voxel to the correlation. This procedure allows to characterize voxels as positive or negative. The former contribute positively to the correlation, as their removal decreases the correlation value; the latter contribute negatively to the correlation, as their removal increases the correlation value.

2.7 | Leave-one-pathology-out

The leave-one-pathology-out is a validation technique used to evaluate both the variability and generalizability of measurements. The procedure for the calculation of the mean Euclidean distance described above was performed several times, each run excluding one of the 26 pathologies included in the study. For all the outcomes resulting from each measurement, the voxel-wise standard deviation was calculated to verify the degree of variability and consistency of the different measurements with regard to each pathology.

3 | RESULTS

3.1 | Maps of mean distance

The map of the mean Euclidean distance of co-alterations related to GM decreases shows higher peaks in the dorsal and anterior regions of the left prefrontal cortex (PFC) and the bilateral medial temporal lobe (MTL). Left posterior insula, left postcentral gyrus, right precentral gyrus, and clusters in the bilateral temporal and occipital lobes are also involved. The map of GM increases is characterized by more extreme values compared to that of GM decreases; thus, despite the low magnitude of many voxels, certain areas reach higher values than those observed in the other map. These areas are the bilateral precentral and postcentral gyri, the right anterior PFC, an inferior cluster in the bilateral occipital cortex, and the left medial cuneus (Figure 3).

The sensorimotor network, the default mode network (DMN), the salience network (SN), the dorsal attention network (DAN), and the thalamus and basal ganglia are the systems where both GM increases and GM decreases show long distance co-alterations. GM decreases show longer distance co-alterations than the GM increases in the auditory network and the cerebellum (Figure 4).

The maps of mean fiber-length and topological distance of co-alteration present both a certain similitude to those of Euclidean distance. Taken together, they highlight the importance of the sensorimotor cortices, the unilateral dorsal anterior PFC (left for the decreases, right for the increases), the occipital cortices, and the temporal lobe (Figure 3). The involvement of the canonical networks in the fiber-length co-alteration maps present some similarities to that showed by the Euclidean maps, although the DMN, the orbitofrontal cortex (OFC), and the Visual Network 1 (V1) present relatively longer mean distance in the fiber-length map. The networks involved in the topological maps are not so different from those of the Euclidean distance maps, but all the visual networks appear to be co-altered with more distant regions, and, for what concerns the decreases, the cerebellum shows shorter distance (Figure 4).

For each area, we also assessed if it tends to be co-altered with regions belonging to the same functional network or to different ones. Specifically, for each area, we assessed its "network-betweenness" as the ratio between its internetwork edges and its total number of edges. The same pattern emerges both with decreases and increases: the associative areas tend to be more within-network co-altered, while the primary regions are those more likely to co-alter with different networks (Figure 4). Exceptions to this trend are the DAN, which shows many internetwork edges, V3, and the sensorimotor network, which show the opposite pattern. The network-betweenness for each network is presented in Table 3. Overall, the internetwork patterns of co-alterations tend to be similar between decreases and increases (Figure 5, Table 3). The network-betweenness of each network was tested against that of 1,000 null Maslov–Sneppen networks (Maslov & Sneppen, 2002), calculated with the Brain Connectivity Toolbox (Rubinov & Sporns, 2010). For what concerns the decreases, all networks were significantly less inter-co-altered than the null model ($p = .01$), with the exception of V1 that was not different from the null model at $p = .05$. Concerning the increase condition, V1 and V2 were not different from the null model at $p = .05$. The remaining networks were significantly less inter-co-altered than the null model ($p = .01$). It is important to stress that such relatively low network-betweenness of co-alteration do not conflict with a finding of long physical distance. In fact, for large network such as the DMN or the SN, a low network-betweenness is perfectly consistent with a high physical distance, and even a high topological one, if we consider that a long-range network could be divided in submodules.

The within-co-alteration of the cerebellum and thalamus-basal-ganglia are other examples of unexpected network-betweenness. In fact, the prevalence of within-network co-alterations in these regions seems to be in contradiction with their supposed low level in the functional hierarchy, as well as with their long mean distances. As for the thalamus-basal-ganglia network, it must be observed that it consists in many nodes, therefore it can have enough long-distance inter-network edges to have long mean distances, and many relatively shorter distance intra-network edges to result in a low network-betweenness. Regarding the cerebellum, many of its nodes form a closed system that does not co-alter with other networks, explaining its strong within-co-alteration. However, a relative minority of its regions is co-altered with many
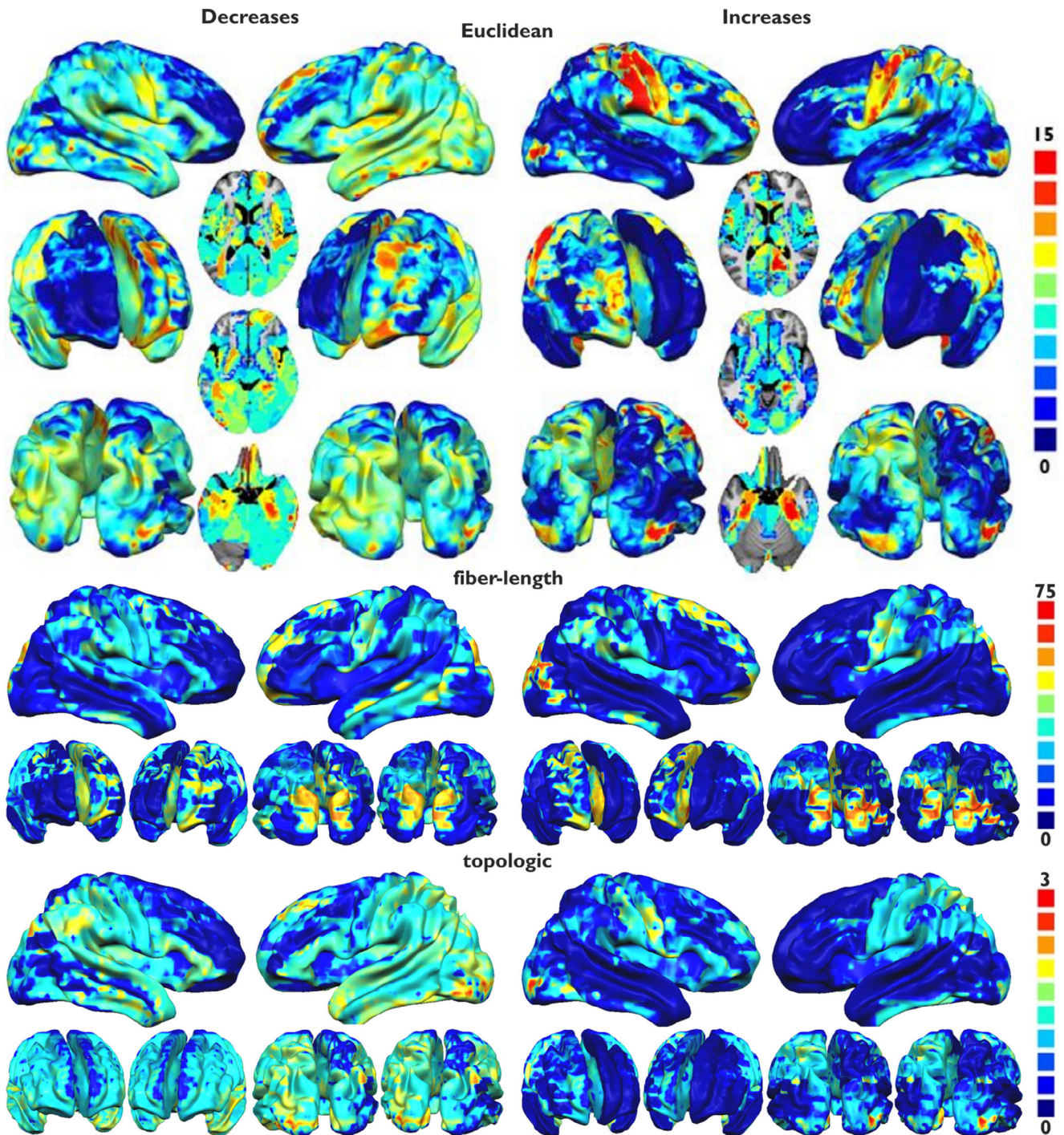
FIGURE 3 Parametric mapping of the mean distances of co-alterations, divided for decreases and increases. Higher values indicate increasing mean distance. Axial slices are in radiological convention

external nodes, especially belonging to the thalamus-basal-ganglia and OFC, justifying its mean long distance (Figure 5).

3.2 | Comparison with the map of functional DC

The co-activation DC map reveals the presence of normative hubs in the bilateral superior temporal cortex, bilateral occipital cortex, right temporoparietal junction, and right inferior prefrontal gyrus. The systems that present the higher DC of co-alterations are the sensorimotor network, the SN, and the auditory network. The correlations between the values of functional DC and those of GM decreases and increases mean Euclidean distance are $r = .54$ and $r = .42$, respectively. The VCC analyses report a high concordance between the functional degree map and both the GM increases and decreases mean distance co-alteration maps in most of the voxels, except for those belonging
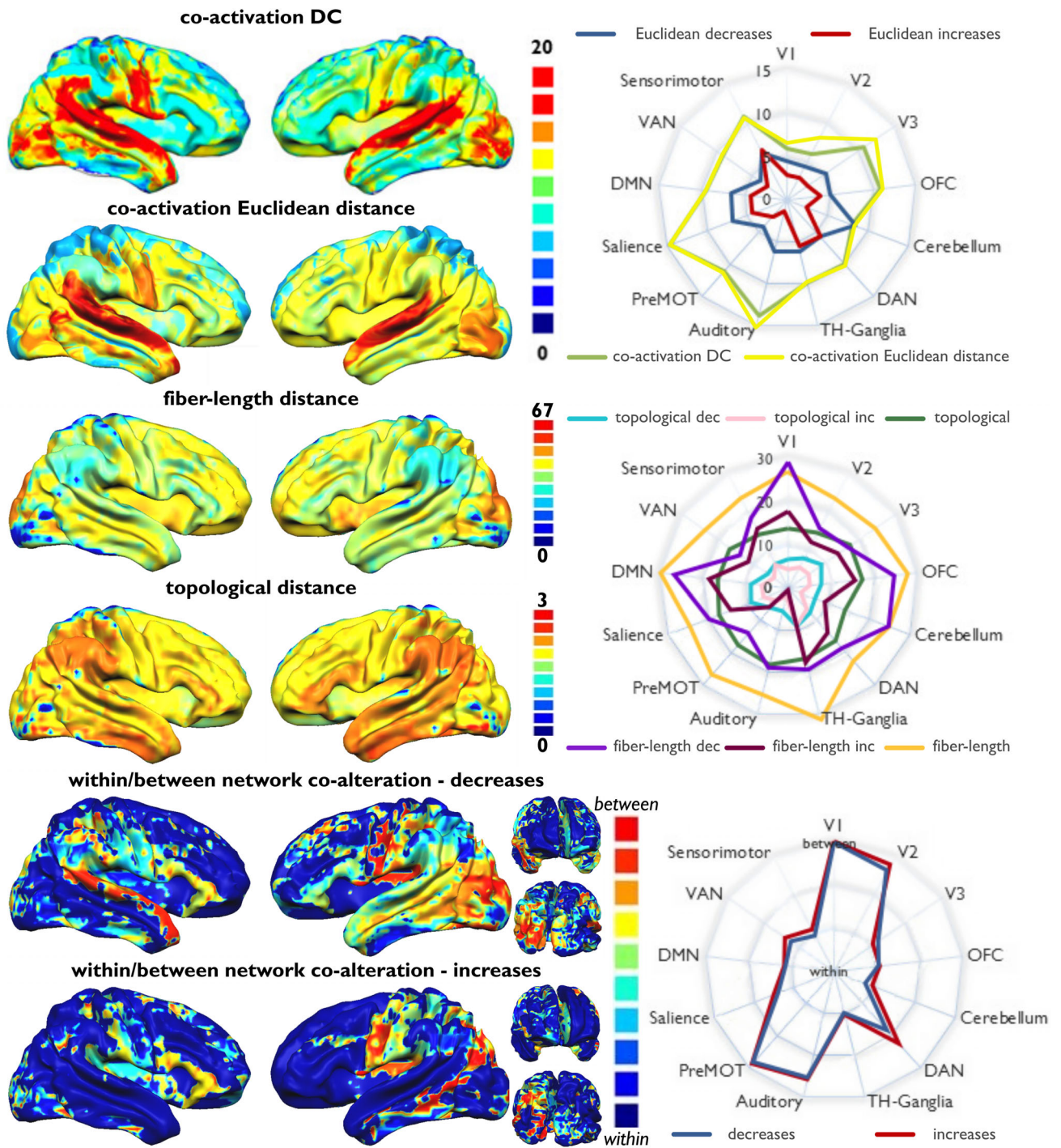
FIGURE 4 Top left panel: Surface mapping of the co-activation degree centrality and mean Euclidean distance. Top right panel: Radar chart comparing the average values of mean Euclidean distances of decreases and increases, mean Euclidean distance, and degree centrality of co-activation for each of the following networks: visual networks 1, 2 and 3 (V1, V2, and V3), orbitofrontal cortex (OFC), cerebellum, dorsal attentional network (DAN), thalamus and basal ganglia, auditory network, premotor network, salience network, default mode network (DMN), ventral attentional network (VAN), and sensorimotor network. Middle left panel: Surface mapping of the mean fiber-length and structural topological distances. Middle right panel: Radar chart comparing the average values of mean fiber-length and topological distances of decreases, increases, and structural connectivity for each canonical network. Bottom left panel: Surface mapping of the network-betweenness (between-network edges/total number of edges. Bottom right panel: Mean network-betweenness for each canonical network
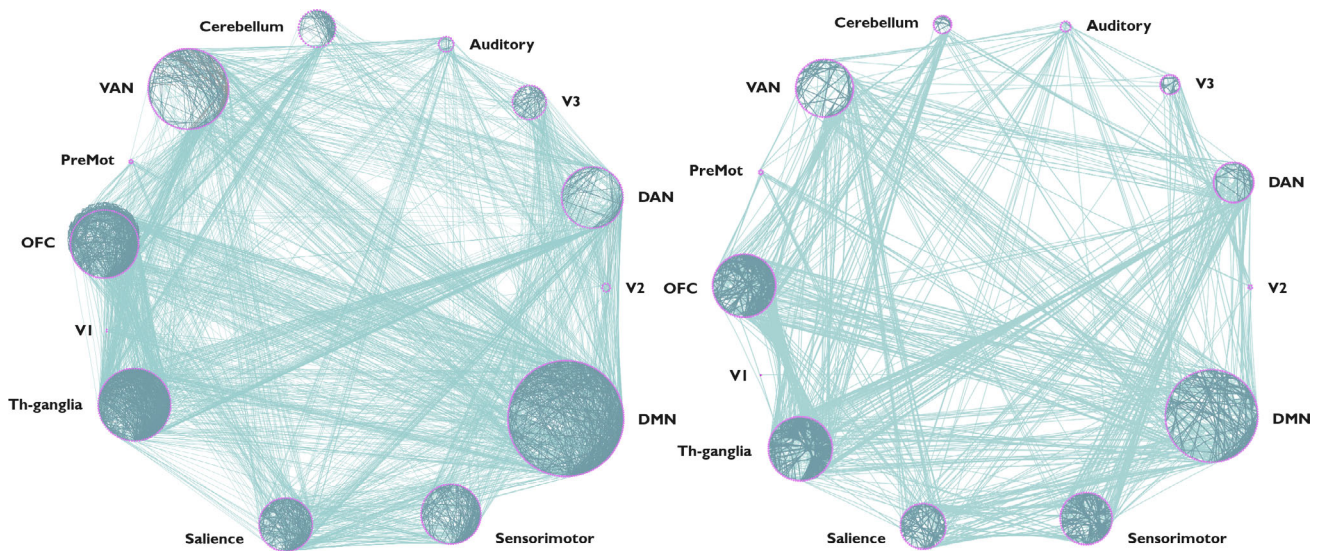
FIGURE 5 Two-dimensional representation of the decreases and increases co-alteration networks, organized according to the belonging of each node to each one of the following resting-state networks: visual networks 1, 2, and 3 (V1, V2, and V3), orbitofrontal cortex (OFC), cerebellum, dorsal attentional network (DAN), thalamus and basal ganglia, auditory network, premotor network, salience network, default mode network (DMN), ventral attentional network (VAN), and sensorimotor network

to the right PFC and the left middle frontal gyrus (MFG) in the GM decreases map, and those belonging to the left PFC, right MFG, and bilateral temporal cortices in the GM increases map (Figure 6).

The map of co-activation mean distance presents hubs in the bilateral superior temporal cortex, in the bilateral occipital cortex, and in the right precentral and postcentral gyri. The mean distance distribution across canonical networks resembles that of the functional DC. The correlation between the values of co-activation mean distance and those of GM decrease and increase are $r = .50$ and $r = .30$, respectively. The VCC results are overall similar to those obtained with the DC map, but they present less concordance. In particular, the VCC map with the increases reveals strong differences in the superior temporal cortices (Figure 6).

The mean fiber-length distance map presents long-distance hubness especially in the occipital lobe and OFC (Figure 4). The correlations between the regional values of this map and the decrease and increase mean fiber-length distances are $r = .63$ (decrease) and $r = .51$ (increase). The correlations of the decrease and increase mean fiber-length distance with the co-activation DC were much lower ($r = .15$ and $r = .17$ respectively). Indeed, the VCC maps show less concordance with such map than the Euclidean distance (Figure 6). Nonetheless, they are distributed in a similar way, with the notable differences that the prefrontal patterns seem to be reversed across the hemispheres for increases and decreases, and that the superior temporal cortices are regions of discordance in this case.

The mean topological distance map presents higher values in the temporal and parietal lobe, and in the inferior frontal gyrus (IFG) (Figure 4). The values of this map correlate with the values of the same measure on the co-alteration networks with $r = .86$ for the decreases and $r = .72$ for the increases. The topological distance produced much higher correlations ($r = .42$ and $r = .44$) with the co-activation DC than

with the fiber-length distance. Despite that, the regions of discordance appear to be much more widespread, with high concordances focused in the thalamus and basal ganglia. Specifically, it seems that a large part of the concordance between the decreases mean topological distance and the co-activation DC is concentrated in the caudate, other than in the occipital lobe (Figure 6).

Table 2 presents all the correlations between the co-alteration and co-activation maps. All the correlations were significant at $p = .01$. Since the Euclidean distance seemed to be the one that performed better, overall, the subsequent analyses were conducted on such measure.

3.3 | Leave-one-pathology-out analysis

The regions with the highest variability across diseases are the bilateral (but especially right) IFG, the bilateral insula, the bilateral temporal lobe, and the bilateral occipital lobe for the map of GM decreases; the right precentral and postcentral gyri, the left MFG, the left angular gyrus, and the right occipital lobe for the map of the GM increases (Figure 7). The two maps involve different systems, especially the sensorimotor network, the DMN, the SN, the auditory network, and the thalamus and basal ganglia for the GM decreases, and the sensorimotor network and V1 for the GM increases (Figure 7).

3.4 | Schizophrenia and Alzheimer's disease

With regard to the map of Euclidean distance of decreases of schizophrenia (Figure 8), the left auditory cortex shows the longest mean distance co-alterations (and, albeit less strongly, the right auditory
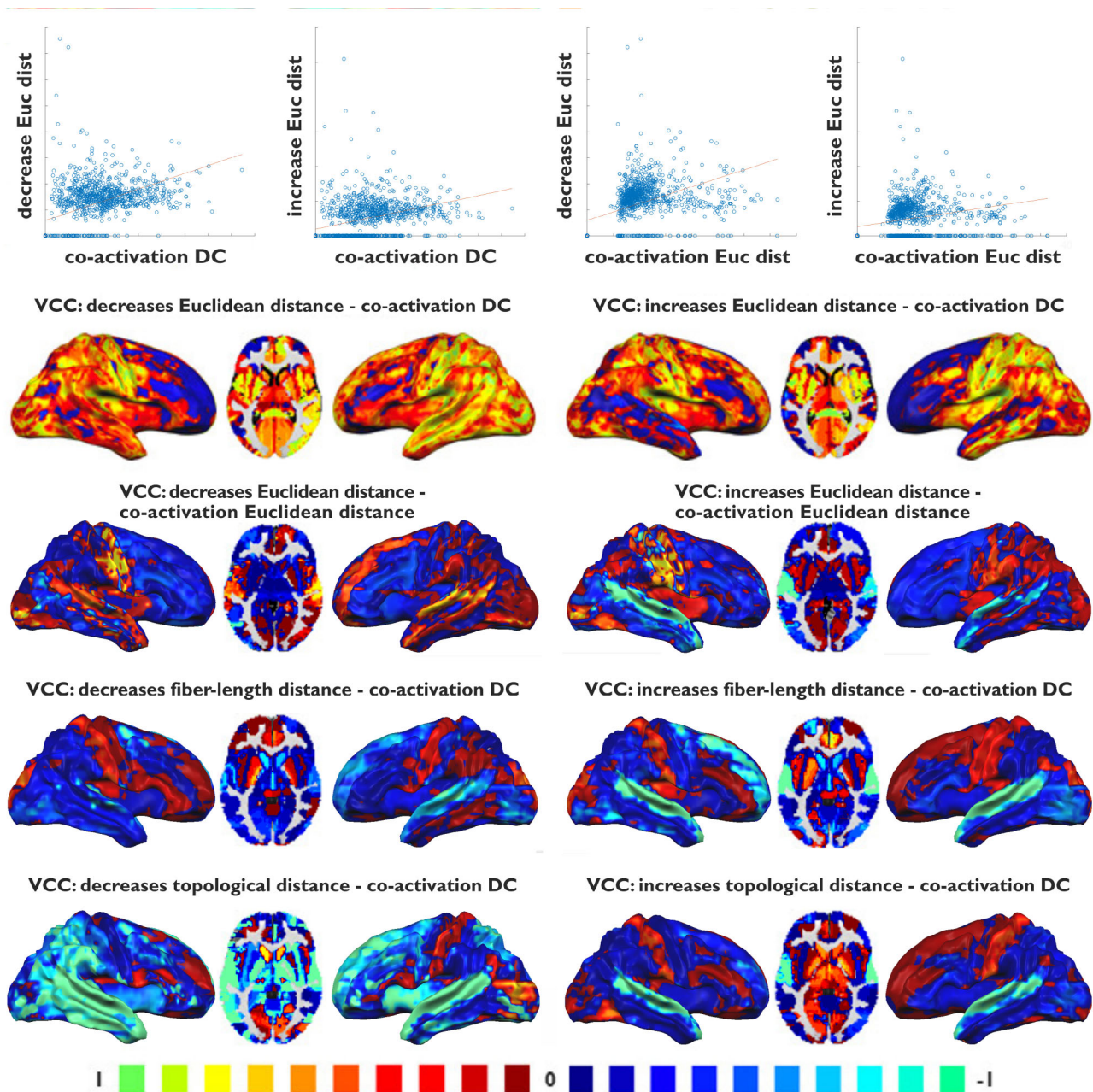
FIGURE 6 Top panel: Scatter plots of co-activation and co-alteration values of each area of the Talairach Daemon atlas. Bottom panel: Parametric mapping of the voxels' contribution to correlation analysis between the functional meta-analytic degree centrality map and the functional meta-analytic mean distance map with the mean distance co-alteration maps of decreases and increases. Positive values indicate areas of concordance between the maps, negative values indicate discordance. Axial slices are in radiological convention

cortex is also involved). Small clusters can be found in the right superior temporal sulcus (STS). The bilateral insula is widely involved, as well as the left IFG (especially in its posterior portion), the bilateral anterior cingulate cortex (ACC), the bilateral OFC and the ventromedial PFC, the MTL (especially the left one), and the bilateral caudate. The ALE map of decreases shows overall comparable results, but it seems to be less sensitive. Significant clusters can be found in the left amygdala, bilateral insula, right caudate head, left posterior IFG, bilateral dorsal ACC and left anterior/ventral ACC, and bilateral OFC (Figure 8). The map of GM

increases shows long distance co-alterations mainly in the basal ganglia, especially in the left putamen. The ALE of increases presents only a small cluster in the left putamen. The correlations between the ALE maps and the corresponding distance maps were $r = .15$ for the decrease condition and $r = .07$ for the decrease condition (calculated with the use of a brain mask; both correlations resulted significant, however, because of the voxel-wise nature of the ALE map, it was not possible to calculate them region by region as the previous ones. Thus, the test results depend on the large number of voxels).

TABLE 2 Pearson's *r* values for all the comparisons between co-alteration and co-activation network measures

Co-alteration network	Control network	Pearson's *r*
Mean Euclidean distance—decrease	Degree centrality—co-activation	.54
	Mean Euclidean distance—co-activation	.50
	Mean fiber-length distance	.36
	Mean topological distance	.38
Mean Euclidean distance—increase	Degree centrality	.44
	Mean Euclidean distance	.30
	Mean fiber-length distance	.29
	Mean topological distance	.31
Mean fiber-length distance—decrease	Degree centrality	.15
	Mean Euclidean distance	.14
	Mean fiber-length distance	.63
	Mean topological distance	.50
Mean fiber-length distance—increase	Degree centrality	.17
	Mean Euclidean distance	.11
	Mean fiber-length distance	.51
	Mean topological distance	.40
Mean topological distance—decrease	Degree centrality	.42
	Mean Euclidean distance	.22
	Mean fiber-length distance	.75
	Mean topological distance	.86
Mean topological distance—increase	Degree centrality	.44
	Mean Euclidean distance	.17
	Mean fiber-length distance	.61
	Mean topological distance	.72

Note: All the correlations are significant at *p* = .01.

With regard to the map of GM decreases of Alzheimer's disease (Figure 9), long Euclidean distance co-alterations characterize the caudate (principally the left one), the MTL (especially the left one), the PCC, the left temporoparietal junction, the left orbital cortex, certain clusters in the bilateral anterior insula, and a cluster in the STS. In turn, the map of GM increases shows long distance co-alterations just in the bilateral MTL (particularly the left one). The correlations between the ALE maps and the corresponding distance map were *r* = .19 for the decrease condition and *r* = .38 for the increase condition (calculated with the use of a brain mask; they both resulted significant, however they were calculated voxel-wise).

4 | DISCUSSION

4.1 | Spatial distribution of the mean distance of co-alterations

This study investigates, for the first time, the spatial distribution of the distance of co-alterations and highlights the capacity of this type of measurement to provide insightful indications about the distribution patterns of GM alterations related to brain diseases. Findings show that the spatial distribution of the mean distance of transdiagnostic co-alterations varies between areas in interesting and meaningful ways.

For instance, an intriguing observation is that the left dorsal and anterior PFC tend to co-alter with distant areas in all the decreases maps. This is confirmed by the high network-betweenness of those areas, as well as the surprisingly high network-betweenness of the DAN compared to other associative cortices (Figure 4, Table 3). In addition, the lateral parts of PFC show low transdiagnostic variance (Figure 7), which means that they present long-range co-alterations related to GM decreases in a wide range of pathologies. This is consistent with the low mean distance variability exhibited by the DAN (Figure 7), as well as with the clinical and anatomical observation of executive functions deficits in many diseases (Goodkind et al., 2015; McTeague, Goodkind, & Etkin, 2016). On the contrary, the left medial anterior PFC, and especially a part of the left medial dorsal PFC, display high variance, thus suggesting that the medial PFC, despite its low mean transdiagnostic distance, may still be involved in long-range co-alterations in several disorders.

It is interesting to observe that all the three maps of mean distance of co-alterations related to the GM increases show higher values in the right hemisphere than in the left, in spite of the left prevalence of the map related to the GM decreases. This difference is particularly evident in the aforementioned dorsal and anterior lateral PFC (Figure 3), and it indicates an intriguing asymmetry in the pathological involvement of the left and right hemispheres, as the two appears to show more global or local patterns of co-alterations in the opposite form of volumetric abnormalities.

The MTL shows long-range co-alterations related to GM decreases, both with Euclidean and topological distance. Given its involvement in memory and learning, it is likely to be co-altered with many other associative areas in a variety of diseases, causing symptoms of memory loss, for instance in neurodegenerative conditions such as Alzheimer's disease, or symptoms of inappropriate memory and limbic responses that are frequently observed in the ruminations characterizing depression (Sheline et al., 2009). Significantly, the MTL is part of the DMN (Andrews-Hanna, Reidler, Sepulcre, Poulin, & Buckner, 2010; Buckner, Andrews-Hanna, & Schacter, 2008), which is one of the most involved brain networks in long-range GM decreases (Figure 4).

Other areas of long-distance co-alterations related to the maps of GM increases (and, to a lesser extent, to those of decreases) are the precentral and postcentral gyri, particularly within the right hemisphere. Indeed, the sensorimotor network is one of the most involved systems in the map of GM increases (Figures 3, 4). However, these
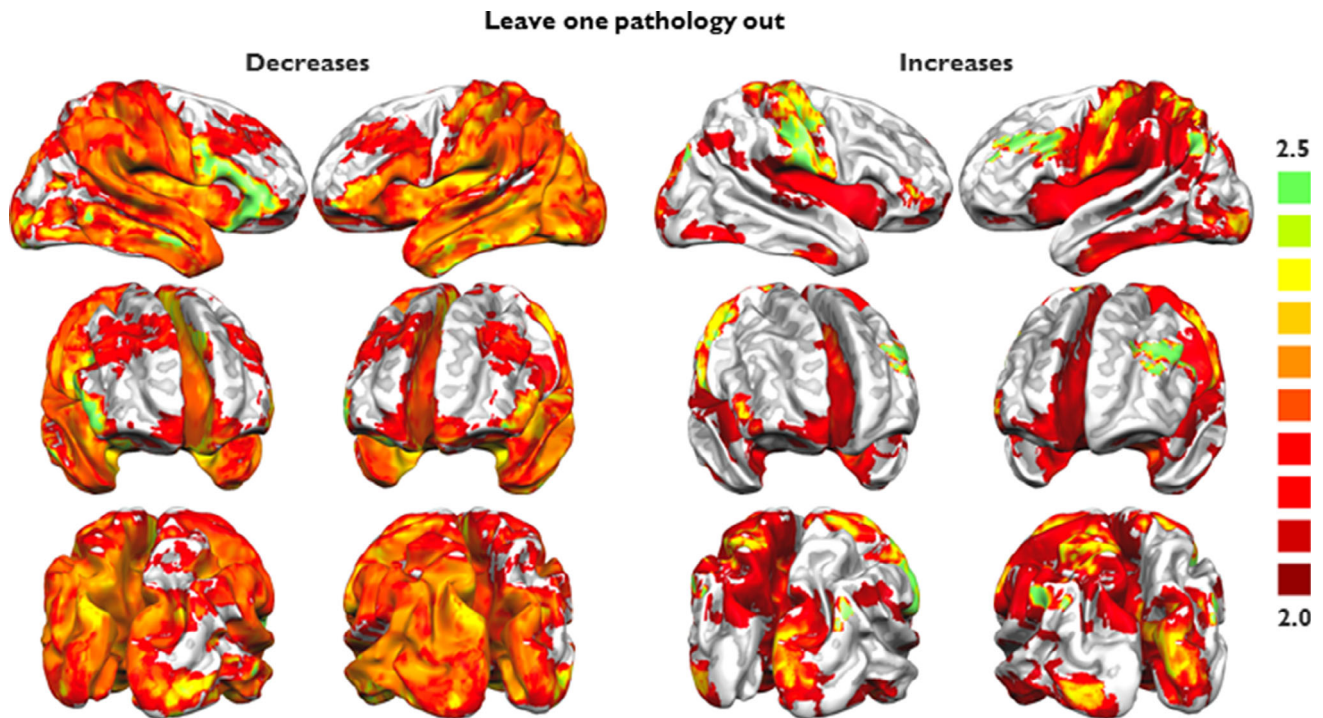
FIGURE 7 Top panel: Surface mapping of the transdiagnostic variance of the mean Euclidean distance maps of decreases and increases. Higher values indicate higher variance, that is, the voxels whose value in the mean distance map is more variable across pathologies

regions are also characterized by high transdiagnostic variance (Figure 7). Therefore, the sensorimotor network exhibits long-distance co-alterations, but its involvement is not consistent across diseases, in contrast to the anterodorsal lateral PFC.

The three different measures of distance produced similar but distinct results. Overall, they all tend to highlight the importance of the dorsolateral PFC, sensorimotor cortices, and, at a certain degree, the occipital lobe. Their relationship is easier to be commented through an analysis of the mean distances of canonical functional networks. For instance, the longer mean distance of the areas belonging to the DMN in the fiber-length and Euclidean maps compared to the topological one (Figure 4) might be explained by the fact that such network cover a vast area of the brain. Thus, a spread within this network, seemingly happening in the Alzheimer disease (Buckner, 2005; Buckner et al., 2009; Iturria-Medina & Evans, 2015), would range across a long physical distance despite travelling along short paths. On the contrary, the longer mean fiber-length distance of the VN1, which has not a particularly large volume, might be better accounted for by a between-network spread.

This hypothesis is confirmed by their proportion of intra-network edges. In fact, the DMN is one of those networks with a strong between-network co-alteration, and the VN1 co-alters more within itself (Figure 4). However, its size seems to be not the only explanation for the "network-betweenness" of co-alteration. In fact, the networks with an associative function tend to be more within-network co-altered, while the areas with primary functions tend to show the opposite trend. Anyway, the size of a network, as well as its placement, is not the result of a case, since they were probably fine-tuned by the evolution to minimize the brain wiring cost (Bullmore & Sporns, 2012). The DMN, for instance,

appears to be located so as to be equidistant from primary cortices (Margulies et al., 2016). In any case, beside this global trend of high network-betweenness for high-hierarchy networks, some intriguing inconsistencies emerge. In particular, the DAN, associated to top-down attention, presents high network betweenness while the opposite is true for the ventral attention network (VAN), associated to bottom-up attention (Corbetta & Shulman, 2002). This is also confirmed by the fact that the DAN has a longer mean distance than the VAN with each of the measures and both in increases and decreases. Such observation provides support for the finding of long-distance hubness of the dorsal PFC.

The network-level analysis allows to highlight the general similarity between the maps of decrease and increase obtained with a given measure of distance, although some exceptions stand out. In fact, the cerebellum and the auditory network tend to have longer mean distance in the decrease maps than in the increase maps. Thus, these areas seem to have the tendency to be co-altered with a set of regions beyond those they are functionally associated. This observation might indicate that the relation between pathology and connectivity can be stricter or relaxed in different part of the brain, and those regions that do not co-alter in accordance with connectivity are those in which the models of spread are less explicative.

4.2 | Comparison of the co-activation and co-alteration maps

The investigation of the relationship between functional centrality and anatomical distance provides evidence for a good convergence between
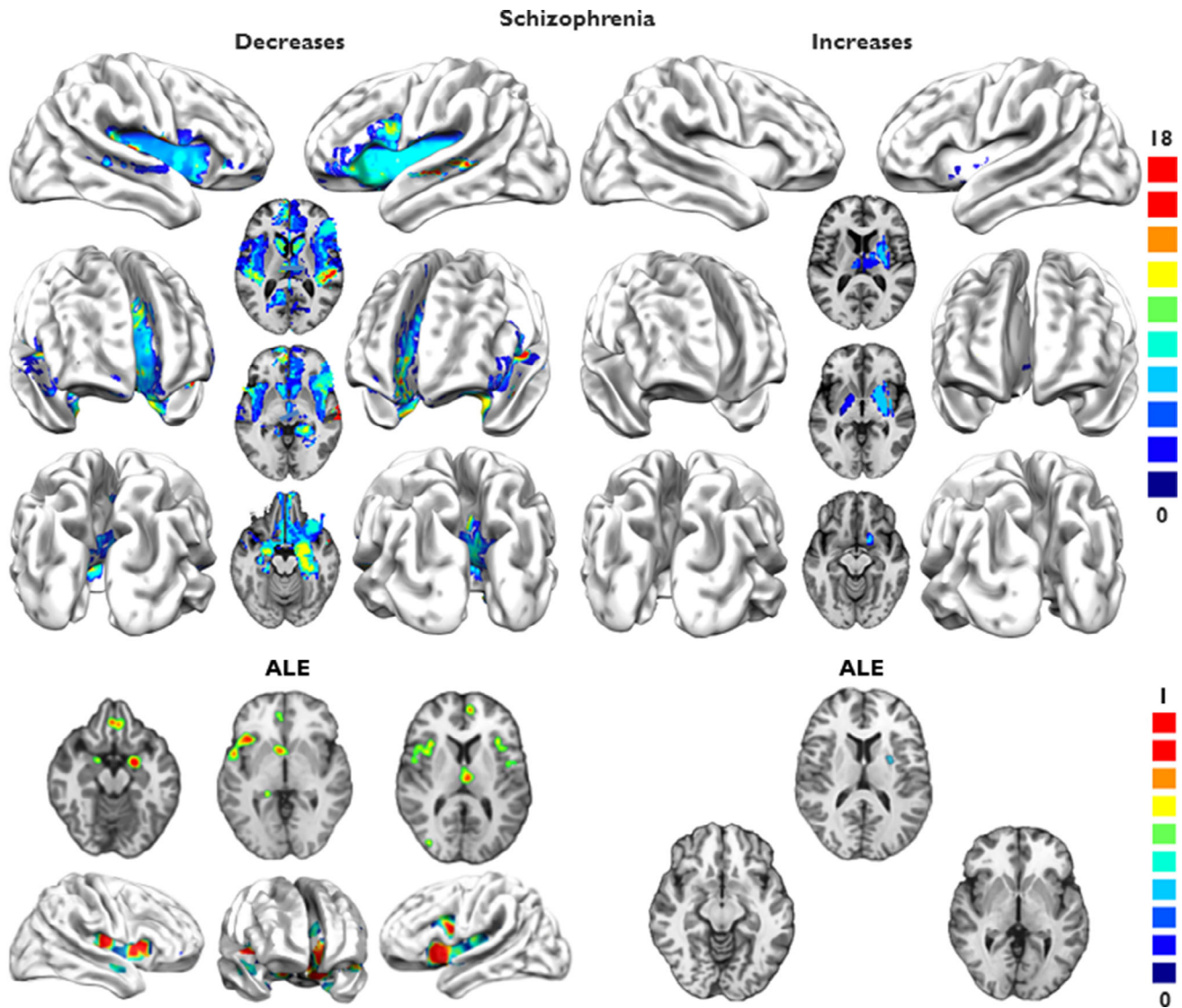
FIGURE 8 Top panel: Parametric mapping of the mean Euclidean distance of co-alterations in schizophrenia, divided for decreases and increases. Higher values indicate increasing mean distance. Bottom panel: Parametric mapping of the anatomical likelihood estimation of decreases and increases of schizophrenia. Axial slices are in radiological convention

the map of co-activation DC and those of Euclidean and topological distance. This strongly suggests that brain functional hubs are also the regions whose mean distance of co-alteration is longer. Save for the right PFC, most of the cortical areas contribute positively to the correlation between functional DC and co-alteration distance. It should be observed that the frontal voxels in the dorsal and anterior PFC displaying low convergence are not those characterized by long transdiagnostic distance. On the contrary, the dorsal and anterior PFC show high convergence between co-activation centrality and co-alteration distance in the left hemisphere for the GM decreases, as well as in the right hemisphere for the GM increases, where long-distance co-alterations are found. In general, regions of long-distance co-alteration, such as the precentral and postcentral gyri and the insula, exhibit high consistency with the map of co-activation centrality (Figure 4). Of note, precentral and postcentral gyri were recently found

to be hubs of long-distance connectivity when short-rage connections are subtracted from the connectome (Esfahlani, Bertolero, Bassett, & Betzel, 2019). The values of co-alteration distance are also correlated with those of co-activation distance, highlighting the relation between pathology and connectivity. This can be seen as a further confirmation of the pathoconnectivity model (Cauda et al., 2019), suggesting that the distribution of the anatomical anomalies could somewhat depend on the normal brain connections.

One of the fundamental issues in the study of co-alterations is to understand the responsible mechanism for morphological covariations of specific sets of areas in relation to a pathological process. Our analyses provide evidence of an interesting association between the distance of co-alterations and the functional DC. As brain hubs are supposed to be preferentially targeted by pathological alterations (Buckner et al., 2009; Crossley et al., 2014; de Haan, Mott, van Straaten,
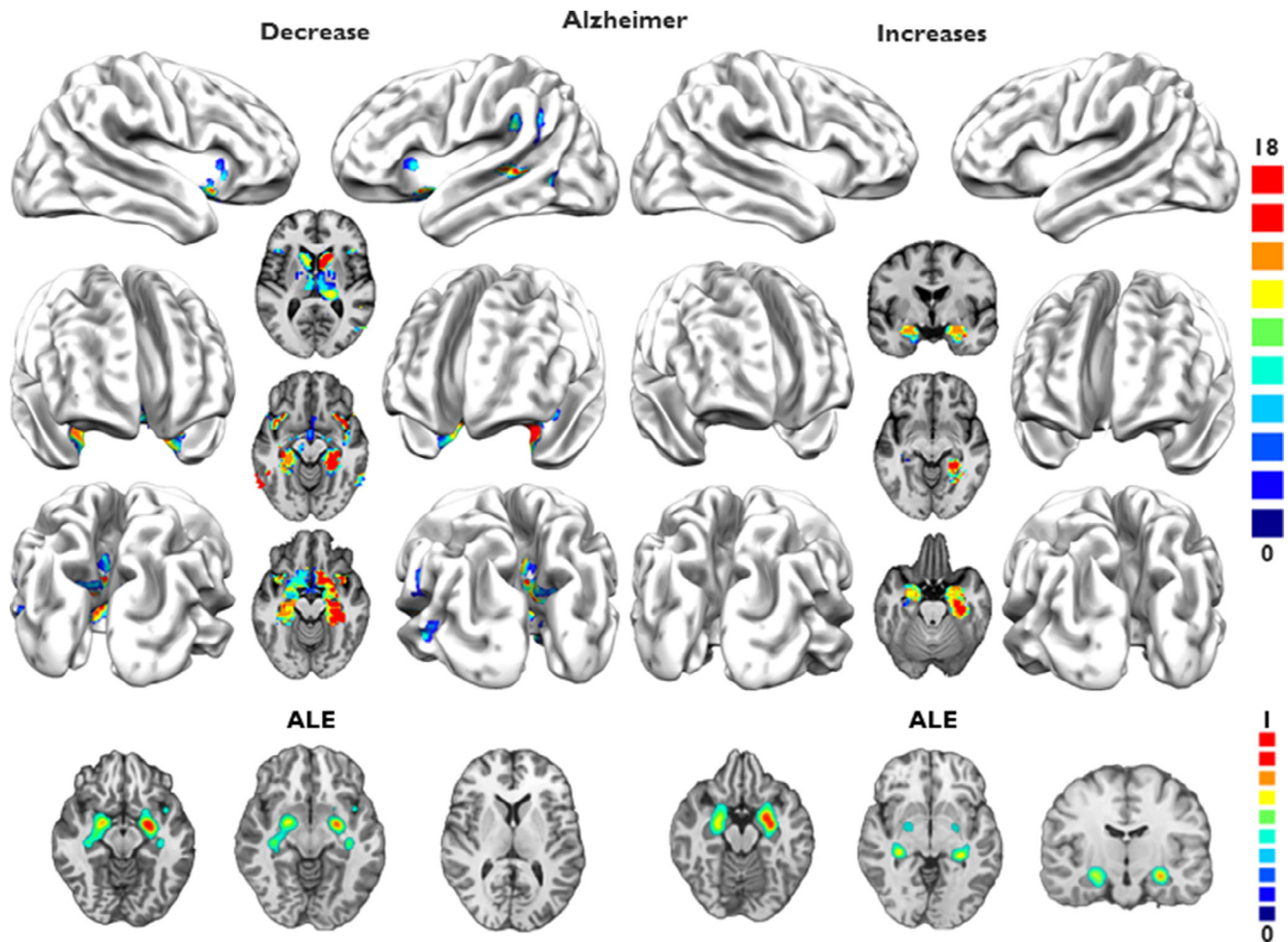
FIGURE 9 Top panel: Parametric mapping of the mean Euclidean distance of co-alterations in Alzheimer's disease, divided for decreases and increases. Higher values indicate increasing mean distance. Bottom panel: Volumetric mapping of the anatomical likelihood estimation of decreases and increases of schizophrenia. Axial and coronal slices are in radiological convention

Scheltens, & Stam, 2012), the finding of a convergence between functional DC distribution and long-distance co-alteration areas suggests that brain regions which are more likely to be affected by diseases are also more likely to be co-altered with distant areas. A possible explanation might be that such regions are more susceptible to metabolic stress in virtue of their numerous connections and intense work of integration of different information (Crossley et al., 2014). Although capable of explaining the high rate of damage undergone by hubs, this model alone fails to explain our findings: it remains unclear why areas of high metabolic stress should be co-altered with other distant regions. Conversely, the transneuronal spread hypothesis (Zhou et al., 2012), which accounts for the pathologic progression with the diffusion of toxic agents such as misfolded proteins, seems to be more up to the task.

The idea that misfolded proteins are responsible for the pathological spread has found several supporting evidence in studies about neurodegenerative diseases (Ahmed et al., 2016; Goedert et al., 2017; Guest et al., 2011; Iturria-Medina, Sotero, Toussaint, & Evans, 2014; Raj, Kuceyeski, & Weiner, 2012; Raj & Powell, 2018; Seeley et al., 2009; Warren et al., 2012; Warren et al., 2013; Zhou et al., 2012), but this has also been putatively extended to psychiatric conditions. Indeed, GM loss

was recently found to be dependent from connectivity in patients with schizophrenia (Shafiei et al., 2019). In fact, insoluble aggregates of disrupted-in-schizophrenia 1 (DISC1) were associated to sporadic cases of schizophrenia, bipolar disorder, and depression (Korth, 2012; Leliveld et al., 2008). In addition, in vitro studies have demonstrated that aggregates of DISC1 are able to transfer between cells via tunneling nanotubes (Zhu, Abounit, Korth, & Zurzolo, 2017). These aggregates can selectively affect dopaminergic brain functioning at presynaptic and postsynaptic level (Dahoun, Trossbach, Brandon, Korth, & Howes, 2017; Tropea, Hardingham, Millar, & Fox, 2018), and, as they are related to oxidative stress (Trossbach et al., 2016), the transneuronal spread hypothesis is not incompatible with the metabolic stress model. On the contrary, both pathological mechanisms might be necessary for a hub to be damaged (Saxena & Caroni, 2011). According to this view, brain hubs are more vulnerable to deterioration, and in turn they can spread the alterations to the connected areas. Furthermore, given their high degree of connectivity and their role of integration of different clusters, hubs are generally linked to many distant regions, and this makes them ideal for spreading pathological alterations along several long-range connections.

TABLE 3 Network-betweenness and total number of edges for each network, in the decrease and increase condition

	Decreases		Increases	
	Network-betweenness	Number of edges	Network-betweenness	Number of edges
V1	1	20	1	2
V2	0.89*	35	0.92	13
V3	0.62*	164	0.53*	71
OFC	0.42*	1056	0.41*	722
Cerebellum	0.49*	202	0.73*	113
DAN	0.71*	386	0.79*	244
Thalamus ganglia	0.20*	1097	0.21*	799
Auditory	0.87*	95	0.81*	26
PreMot	0.79*	14	0.83*	12
Salience	0.40*	432	0.44*	226
DMN	0.37*	1098	0.49*	403
VAN	0.52*	513	0.67*	255
Sensorimotor	0.29*	352	0.33*	299
Total	0.58*	5464	0.63*	3185

Note: An asterisk indicate the network-betweennesses significantly inferior than the null model at $p = .01$. The network-betweenness is calculated as the ratio between the number of internetwork edges and the total number of edges. Similarly, the total network-betweenness is calculated as the ratio between all the internetwork edges and the total number of edges.

Abbreviations: DAN, dorsal attention network; DMN, default mode network; OFC, orbitofrontal cortex; V1, Visual Network 1; VAN, ventral attention network.

It has also been suggested that alterations could propagate by means of a trophic factor release failure (Fornito, Zalesky, & Breakspear, 2015). In other words, the areas connected to the damaged region might suffer morphological GM decreases because they cease to receive trophic factors from them (Chao, 2003), or they might reduce their activity because of the lack of inputs, which could disrupt their activity-dependent synthesis and release of trophic factors (Blöchl & Thoenen, 1995; Gall & Isackson, 1989; Kohara, Kitamura, Morishima, & Tsumoto, 2001), thus leading to a cascade of anatomical decreases. A disruption of the balance of the trophic mechanism, in form of an enhanced trophic release or a lack of growth-inhibitory signals (Perlson, Maday, M meng, Moughamian, & Holzbaur, 2010), may also account for the generations of networks of GM increases. Of course, the effect of morphometric increase might be of iatrogenic nature (Hafeman, Chang, Garrett, Sanders, & Phillips, 2012; Navari & Dazzan, 2009), although this general explanation does not consider the similarity between hubs of long-distance increase to that of FC. Thus, we suggest that a mixture of metabolic stress, toxic spread, trophic factor release disruption, and shared vulnerability to genetic and environmental factors influence the distribution of both decrease and increase co-alteration along connectivity pathways (Cauda et al., 2019). Therefore, brain hubs might be not only extremely vulnerable to disorders but also substantially responsible for the long-range spread of morphological changes.

The comparison of the three maps of mean distance suggests some interesting speculations. First of all, the Euclidean and topological maps are more consistent with the co-activation DC map than the fiber-length distance, which correlates poorly with the regional hubness (Figure 6). We interpret this observation as the incapability of the fiber-length distance to recapitulate all the factors explaining the co-alterations. While

the Euclidean distance is known to have an effect on connectivity (Bellec et al., 2006; Salvador et al., 2005) and the topological distance reflects an epidemiologic approach to the spread (Raj & Powell, 2018), the fiber-length distance might be unable to model several aspects of pathology. This is in contrast with the findings of Pandya et al. (2019), who report that fiber-length and Euclidean distance are both correlated the Parkinson's disease atrophy. It might be that the fiber-length distance, although not completely adequate to explain many diseases that constitute our database, is proficient to model neurodegenerative disorders. In fact, we found the fiber-length distance of co-alteration to be strongly correlated with the fiber-length distance of co-activation. We interpret this observation as a close correspondence between that part of the co-alteration that can be accounted for by the axonal length (i.e., the toxic spread factor) and normative connectivity.

In fact, we do not postulate that the co-alterations are influenced only by the toxic spread model, nor that they exactly replicate the normal connectivity, because they could be modulated by genetic and environmental factors as well. Thus, the good concordance of the co-alteration Euclidean distance with the co-activation DC could indicate that a more general measure of distance, which does not imply a concept of spread rigidly, makes the model more fit to describe the multifactorial model that might underlie our transdiagnostic "pathoconnectome".

4.3 | Analyses of schizophrenia and Alzheimer's disease

With regard to schizophrenia (Figure 8), areas with long-distance co-alterations of GM decreases have auditory and linguistic roles, a

finding that is in accordance with the auditory hallucinations affecting a portion of these patients (García-Martí et al., 2008; Modinos et al., 2009; Neckelmann et al., 2006; Plaze et al., 2006). Also the caudate and the MTL, as well as other SN regions, exhibit long-distance co-alterations, which is in line with the involvement of this network in the disease (Cauda, Nani, Costa, et al., 2018; Guo et al., 2014; Kapur, 2003; Liddle et al., 2016; Manoliu et al., 2014; Palaniyappan, 2019; Palaniyappan & Liddle, 2012; Palaniyappan, White, & Liddle, 2013; Uddin, 2015; White, Joseph, Francis, & Liddle, 2010). The ALE was able to replicate the alterations in the SN regions but failed to return clusters in the auditory cortices as well as in the caudate. This supports the notion that the distance of co-alteration is more able to individuate clinically relevant regions than the localization of alteration. Long co-alterations of GM increases are found especially in the left putamen, which is coherent with a study that found an increased putamen characterized by leftward asymmetry in schizophrenic patients (Okada et al., 2016) and with our ALE results.

With regard to Alzheimer's disease (Figure 9), long-distance co-alterations of GM increases and GM decreases are found especially in the left hippocampal formation, which is consistent with the assumption that the hippocampus may be the pathological epicenter, as well as with the observation that the left hemisphere is more affected than the right one (Braak, Braak, & Bohl, 1993; Buckner, 2005; Janke et al., 2001; Loewenstein et al., 1989; Manuello et al., 2018; Pievani, de Haan, Wu, Seeley, & Frisoni, 2011; Thompson et al., 2001; Thompson et al., 2003; Thompson et al., 2007). This leftward lateralization was confirmed by the ALE maps; however, the distance maps showed much more areas, such as the PCC and the temporoparietal junction. Those regions are nodes of the DMN, known to be involved in the disease (Buckner, 2005; Buckner et al., 2009; Iturria-Medina & Evans, 2015). Other regions with long-distance co-alterations of GM decreases are the caudate and the insula, with a major involvement in the left hemisphere. The finding that the left MTL is involved in long-distance co-alterations both of GM increases and of GM decreases is intriguing, and might be putatively explained by the effect of compensation, as if this region, in a certain stage of the disease, could be engaged in a system of increases that tries to counteract the damages induced by the disease.

In light of these considerations, the measurement of the mean distance of co-alterations can identify clinically relevant areas, as they are associated with typical symptoms of brain disorders, and even the epicenters of pathological diffusion. In this regard, it should be emphasized that our analysis showed to be more able than a canonical ALE to detect significant effects in those areas. Therefore, our findings advocate in favor of the co-alteration pathoconnectome as a useful tool in the understanding of brain pathology.

4.4 | Limitations

A possible limitation of our analyses is that nodes were defined on the basis of an anatomical atlas; therefore, they may fail to account for more fine-grained distinctions in heterogeneous regions. This choice

aimed to achieve a higher statistical power, as a voxel-wise technique may leave some voxels uncovered by a sufficient number of samples. It could be argued that in a parcellation, the size of the regions of interest (ROIs) determines the minimum spatial resolution for the detection of a hub, but the use of a parcellation with small volumes would have reduced the statistical power in underrepresented brain regions. We therefore chose to use an atlas that previously proved to fit the functional connectivity better than artifactual parcellations (Mancuso et al., 2019). Still, choosing a different anatomical atlas might have produced slightly divergent results.

Another possible consequence of the use of an anatomical atlas compared to a homogeneous parcellation is that the centroid of a large region will be more distant from its neighbor than that of a small region. However, we decided to favor the realism of the network rather than to avoid a bias in the distance of neighbor nodes. Another bias that might affect the co-alteration of neighboring regions comes from the possibility that if a focus of alteration falls on the border between two volumes, both areas will appear as altered. This can be seen as a desired effect in the sense that it would represent the case in which an alteration is shared between two regions. However, it might be argued that, in some circumstances, it could be a rather simplistic model, inducing artifactual close-distance co-alterations. Nevertheless, it must be kept in mind that our study averages the distance of all the significant edges of a node, thus any possible bias in neighboring co-alterations could have only a tenuous effect on the results.

Our research relies only on the VBM BrainMap database, so the generalizability of the results might be limited by any shortcoming of the VBM technique. For instance, the predominance of the hippocampus in the Alzheimer's disease maps might depend on such methodological issue. Although small posteromedial cortical clusters can be appreciated in the map of GM decreases (Figure 9), the absence of large significant neocortical clusters might be due to the modest sensitivity of VBM to changes in the cortical ribbon compared to those in the hippocampal region (Diaz-De-Grenu et al., 2014). Future studies using, for instance, cortical thickness, might extend the validity of the present findings. Another limitation concerns the practical unfeasibility to derive from the BrainMap repository data about the medication status of the large database of patients that entered this meta-analysis. Moreover, our search did not differentiate between gender and age. Therefore, analyses were unable to evaluate the effects of such variables on measuring the mean physical distance of co-alterations. Given the effect of some psychotropic drug of GM volume (Hafeman et al., 2012; Navari & Dazzan, 2009), and that age and sex have been recently reported to be associated with asymmetries in cortical thickness (Guadalupe et al., 2017; Kong et al., 2018), it could be worth investigating how the symmetry of the maps of mean physical distance of co-alterations related to GM increases and GM decreases can differ with respect to these variables.

Finally, we chose the Euclidean distance as main measure in our research, although, such distance between two adjacent cortical areas would cut across an eventual sulcus dividing them, thus underestimating their distance. Such problem could be overcome using geodesic distance; however, this metric will dramatically overestimate the distance

between distant areas. Moreover, the Euclidean distance has been previously used to assess the impact of distance on functional connectivity (Sepulcre et al., 2010), thus we preferred to implement a method in line with this previous research.

4.5 | Future directions

The theoretical position underlying the present study was that the anatomical modifications induced by a disease were better accounted for if seen as interconnected between each rather than as isolated phenomena. Our claims are supported by the better sensitivity our method has, compared to the ALE, to individuate clinically relevant brain regions in the disease-specific analyses. Therefore, future research might adopt a co-alteration approach, using measures such as the mean distance to investigate the anatomical patterns of brain pathology. For instance, the meta-analytic co-alteration hubs can be used as ROIs in a study with native data, observing if the GM alterations in such hubs might be a better predictor of clinical or functional deficits than that of other regions.

Additionally, confirming the hypothesis that the hubs of co-alteration distance were consistent with those of co-activation, this research further substantiated a model of network degeneration. Furthermore, it provided some evidence in favor of a multifactorial approach to pathoconnectivity, highlighting the fact that the simple spread of toxic agents is not sufficient to account for the distribution of alterations. Thus, future studies might focus on disambiguating the contribution of toxic spread, trophic failure, metabolic stress, and shared vulnerability of different diseases. For instance, neurodegenerative damages might be better explained by models of spread, and thus fit better normative connectivity, while neurodevelopmental alterations might be more easily explained by co-occurrences of gene expressions.

5 | CONCLUSION

The theoretical and methodological aim of this article was to substantiate the network degeneration hypothesis and to suggest the usefulness of the notion of co-alteration. Nonetheless, it also produced a series of concrete findings about brain pathology.

First, it showed that, when the brain is affected by a pathological process, the anterior and dorsal PFC tend to be involved long-distance and inter-network co-alterations, thereby this region is to be considered as a key hub of pathology. Second, it illustrated that long-range associative functional networks, with the notable exception of the DAN, tend to constitute paths of intra-network co-alterations. Third, areas of the left hemisphere were revealed to be prevalently co-altered in GM decreases, while areas of the right hemisphere appear to be more co-altered in GM increases. This suggests that the two sides of the brain are differently affected by pathological processes.

Thus, the present work provides evidence that brain hubs are involved in long-range co-alterations. However, it also shows that the

areas whose alterations are coupled with those of distant regions are not the same in all the diseases, suggesting that the patterns of co-alteration might be pathology specific. The mean physical distance of co-alteration, therefore, proves itself to be a useful index capable of providing new insights into the distribution patterns of morphological alterations caused by brain disorders.

CONFLICT OF INTEREST

The authors declare no potential conflict of interest.

DATA AVAILABILITY STATEMENT

Data used in this meta-analysis were obtained from BrainMap (http://brainmap.org/), a publicly available database.

ORCID

Lorenzo Mancuso https://orcid.org/0000-0002-5529-5040
Tommaso Costa https://orcid.org/0000-0002-0822-862X

REFERENCES

Achard, S., Salvador, R., WhAchard, S., Salvador, R., Whitcher, B., Suckling, J., & Bullmore, E. (2006). A resilient, low-frequency, small-world human brain functional network with highly connected association cortical hubs. *The Journal of Neuroscience, 26*, 63–72. http://www.jneurosci.org/cgi/doi/10.1523/JNEUROSCI.3874-05.2006

Ahmed, R. M., Devenney, E. M., Irish, M., Ittner, A., Naismith, S., Ittner, L. M., … Kiernan, M. C. (2016). Neuronal network disintegration: Common pathways linking neurodegenerative diseases. *Journal of Neurology, Neurosurgery, and Psychiatry, 87*, 1234–1241.

Alexander-Bloch, A. F., Vértes, P. E., Stidd, R., Lalonde, F., Clasen, L., Rapoport, J., … Gogtay, N. (2013). The anatomical distance of functional connections predicts brain network topology in health and schizophrenia. *Cerebral Cortex, 23*, 127–138.

Andrews-Hanna, J. R., Reidler, J. S., Sepulcre, J., Poulin, R., & Buckner, R. L. (2010). Functional-anatomic fractionation of the brain's default network. *Neuron, 65*, 550–562. https://doi.org/10.1016/j.neuron.2010.02.005

Bassett, D. S., Bullmore, E., Verchinski, B. A., Mattay, V. S., Weinberger, D. R., & Meyer-Lindenberg, A. (2008). Hierarchical organization of human cortical networks in health and schizophrenia. *The Journal of Neuroscience, 28*, 9239–9248. http://www.jneurosci.org/cgi/doi/10.1523/JNEUROSCI.1929-08.2008

Bellec, P., Perlbarg, V., Jbabdi, S., Pélégrini-Issac, M., Anton, J. L., Doyon, J., & Benali, H. (2006). Identification of large-scale networks in the brain using fMRI. *NeuroImage, 29*, 1231–1243.

Blöchl, A., & Thoenen, H. (1995). Characterization of nerve growth factor (NGF) release from hippocampal neurons: Evidence for a constitutive and an unconventional sodium-dependent regulated pathway. *The European Journal of Neuroscience, 7*, 1220–1228.

Braak, H., Braak, E., & Bohl, J. (1993). Staging of Alzheimer-related cortical destruction. *European Neurology, 33*, 403–408. https://www.karger.com/Article/FullText/116984

Buckholtz, J. W., & Meyer-Lindenberg, A. (2012). Psychopathology and the human connectome: Toward a transdiagnostic model of risk for

mental illness. *Neuron*, *74*, 990–1004. https://doi.org/10.1016/j.neuron.2012.06.002

Buckner, R. L. (2005). Molecular, structural, and functional characterization of Alzheimer's disease: Evidence for a relationship between default activity, amyloid, and memory. *The Journal of Neuroscience*, *25*, 7709–7717.

Buckner, R. L., Andrews-Hanna, J. R., & Schacter, D. L. (2008). The brain's default network: Anatomy, function, and relevance to disease. *Annals of the New York Academy of Sciences*, *1124*, 1–38.

Buckner, R. L., Sepulcre, J., Talukdar, T., Krienen, F. M., Liu, H., Hedden, T., … Johnson, K. A. (2009). Cortical hubs revealed by intrinsic functional connectivity: Mapping, assessment of stability, and relation to Alzheimer's disease. *The Journal of Neuroscience*, *29*, 1860–1873. http://www.jneurosci.org/cgi/doi/10.1523/JNEUROSCI.5062-08.2009

Bullmore, E., & Sporns, O. (2012). The economy of brain network organization. *Nature Reviews. Neuroscience*, *13*, 336–349.

Cauda, F., Costa, T., Nani, A., Fava, L., Palermo, S., Bianco, F., … Keller, R. (2017). Are schizophrenia, autistic, and obsessive spectrum disorders dissociable on the basis of neuroimaging morphological findings?: A voxel-based meta-analysis. *Autism Research*, *10*, 1079–1095.

Cauda, F., Costa, T., Palermo, S., D'Agata, F., Diano, M., Bianco, F., … Keller, R. (2014). Concordance of white matter and gray matter abnormalities in autism spectrum disorders: A voxel-based meta-analysis study. *Human Brain Mapping*, *35*, 2073–2098.

Cauda, F., Costa, T., Torta, D. M. E., Sacco, K., D'Agata, F., Duca, S., … Vercelli, A. (2012). Meta-analytic clustering of the insular cortex. Characterizing the meta-analytic connectivity of the insula when involved in active tasks. *NeuroImage*, *62*, 343–355. http://linkinghub.elsevier.com/retrieve/pii/S105381191200393X

Cauda, F., Mancuso, L., Nani, A., Costa, T., Darby, R. R., Fox, M. D., … Costa, T. (2019). Heterogeneous neuroimaging findings, damage propagation and connectivity: An integrative view. *Brain*, *142*, 1–3. https://academic.oup.com/brain/advance-article/doi/10.1093/brain/awz080/5419302

Cauda, F., Nani, A., Costa, T., Palermo, S., Tatu, K., Manuello, J., … Keller, R. (2018). The morphometric co-atrophy networking of schizophrenia, autistic and obsessive spectrum disorders. *Human Brain Mapping*, *39*, 1898–1928.

Cauda, F., Nani, A., Manuello, J., Premi, E., Palermo, S., Tatu, K., … Costa, T. (2018). Brain structural alterations are distributed following functional, anatomic and genetic connectivity. *Brain*, *141*, 3211–3232. https://doi.org/10.1093/brain/awy252

Chao, M. V. (2003). Neurotrophins and their receptors: A convergence point for many signalling pathways. *Nature Reviews. Neuroscience*, *4*, 299–309.

Corbetta, M., & Shulman, G. L. (2002). Control of goal-directed and stimulus-driven attention in the brain. *Nature Reviews. Neuroscience*, *3*, 201–215.

Crossley, N. A., Mechelli, A., Scott, J., Carletti, F., Fox, P. T., Mcguire, P., & Bullmore, E. T. (2014). The hubs of the human connectome are generally implicated in the anatomy of brain disorders. *Brain*, *137*, 2382–2395.

Dahoun, T., Trossbach, S. V., Brandon, N. J., Korth, C., & Howes, O. D. (2017). The impact of Disrupted-in-Schizophrenia 1 (DISC1) on the dopaminergic system: A systematic review. *Translational Psychiatry*, *7*, e1015–e1015. https://doi.org/10.1038/tp.2016.282

de Haan, W., Mott, K., van Straaten, E. C. W., Scheltens, P., & Stam, C. J. (2012). Activity dependent degeneration explains hub vulnerability in Alzheimer's disease. *PLoS Computational Biology*, *8*(8), e1002582. http://dx.doi.org/10.1371/journal.pcbi.1002582

Diaz-De-Grenu, L. Z., Acosta-Cabronero, J., Chong, Y. F. V., Pereira, J. M. S., Sajjadi, S. A., Williams, G. B., & Nestor, P. J. (2014). A brief history of voxel-based grey matter analysis in Alzheimer's disease. *Journal of Alzheimer's Disease*, *38*, 647–659.

Eickhoff, S., Laird, A., Grefkes, C., Wang, L. E., Zilles, K., & Fox, P. T. (2009). Coordinate-based ALE meta-analysis of neuroimaging data: a random-effects approach based on empirical estimates of spatial uncertainty. *Human Brain Mapping*, *30*, 2907–2926. http://www.ncbi.nlm.nih.gov/pmc/articles/PMC2872071/

Eickhoff, S. B., Bzdok, D., Laird, A. R., Kurth, F., & Fox, P. T. (2012). Activation likelihood estimation revisited. *NeuroImage*, *59*, 2349–2361.

Eickhoff, S. B., Jbabdi, S., Caspers, S., Laird, A. R., Fox, P. T., Zilles, K., & Behrens, T. E. J. (2010). Anatomical and functional connectivity of cytoarchitectonic areas within the human parietal operculum. *The Journal of Neuroscience*, *30*, 6409–6421. http://www.jneurosci.org/cgi/doi/10.1523/JNEUROSCI.5664-09.2010

Eickhoff, S. B., Nichols, T. E., Laird, A. R., Hoffstaedter, F., Amunts, K., Fox, P. T., … Eickhoff, C. R. (2016). Behavior, sensitivity, and power of activation likelihood estimation characterized by massive empirical simulation. *NeuroImage*, *137*, 70–85. http://linkinghub.elsevier.com/retrieve/pii/S1053811916300337

Esfahlani FZ, Bertolero M, Bassett D, Betzel R (2019) Space-independent community and hub structure of functional brain networks. bioRxiv:590935. https://www.biorxiv.org/content/10.1101/590935v1.

Evans, A. C. (2013). Networks of anatomical covariance. *NeuroImage*, *80*, 489–504. https://doi.org/10.1016/j.neuroimage.2013.05.054

Fornito, A., Zalesky, A., & Breakspear, M. (2015). The connectomics of brain disorders. *Nature Reviews. Neuroscience*, *16*, 159–172. https://doi.org/10.1038/nrn3901

Fox, P. T., Laird, A. R., Fox, S. P., Fox, P. M., Uecker, A. M., Crank, M., … Lancaster, J. L. (2005). BrainMap taxonomy of experimental design: Description and evaluation. *Human Brain Mapping*, *25*, 185–198.

Fox, P. T., & Lancaster, J. L. (2002). Mapping context and content: The BrainMap model. *Nature Reviews. Neuroscience*, *3*, 319–321.

Gall, C. M., & Isackson, P. J. (1989). Limbic seizures increase neuronal production of messenger RNA for nerve growth factor. *Science*, *245* (4919), 758–761.

García-Martí, G., Aguilar, E. J., Lull, J. J., Martí-Bonmatí, L., Escartí, M. J., Manjón, J. V., … Sanjuán, J. (2008). Schizophrenia with auditory hallucinations: A voxel-based morphometry study. *Progress in Neuro-Psychopharmacology & Biological Psychiatry*, *32*, 72–80.

Goedert, M., Masuda-Suzukake, M., & Falcon, B. (2017). Like prions: The propagation of aggregated tau and α-synuclein in neurodegeneration. *Brain*, *140*, 266–278.

Goodkind, M., Eickhoff, S. B., Oathes, D. J., Jiang, Y., Chang, A., Jones-Hagata, L. B., … Etkin, A. (2015). Identification of a common neurobiological substrate for mental illness. *JAMA Psychiatry*, *72*, 305–315. http://www.ncbi.nlm.nih.gov/pubmed/25651064

Green, S., Higgins, J. P., Alderson, P., Clarke, M., Mulrow, C. D., & Oxman, A. D. (2008). Introduction. In J. P. Higgins & S. Green (Eds.), *Cochrane handbook for systematic reviews of interventions* (pp. 1–9). Chichester, UK: John Wiley & Sons, Ltd. http://doi.wiley.com/10.1002/9780470712184

Guadalupe, T., Mathias, S. R., vanErp, T. G. M., Whelan, C. D., Zwiers, M. P., Abe, Y., … Francks, C. (2017). Human subcortical brain asymmetries in 15,847 people worldwide reveal effects of age and sex. *Brain Imaging and Behavior*, *11*, 1497–1514.

Guest, W. C., Silverman, J. M., Pokrishevsky, E., O'Neill, M. A., Grad, L. I., & Cashman, N. R. (2011). Generalization of the prion hypothesis to other neurodegenerative diseases: An imperfect fit. *Journal of Toxicology and Environmental Health, Part A*, *74*, 1433–1459. http://www.tandfonline.com/doi/abs/10.1080/15287394.2011.618967

Guo, S., Palaniyappan, L., Yang, B., Liu, Z., Xue, Z., & Feng, J. (2014). Anatomical distance affects functional connectivity in patients with schizophrenia and their siblings. *Schizophrenia Bulletin*, *40*, 449–459. https://academic.oup.com/schizophreniabulletin/article-lookup/doi/10.1093/schbul/sbt163

Hafeman, D. M., Chang, K. D., Garrett, A. S., Sanders, E. M., & Phillips, M. L. (2012). Effects of medication on neuroimaging findings in bipolar disorder: An updated review. *Bipolar Disorders*, *14*, 375–410.

He, Y., Chen, Z. J., & Evans, A. C. (2007). Small-world anatomical networks in the human brain revealed by cortical thickness from MRI. *Cerebral Cortex*, *17*, 2407–2419.

Iturria-Medina, Y., & Evans, A. C. (2015). On the central role of brain connectivity in neurodegenerative disease progression. *Frontiers in Aging Neuroscience*, 7, 1–10.

Iturria-Medina, Y., Sotero, R. C., Toussaint, P. J., & Evans, A. C. (2014). Epidemic spreading model to characterize misfolded proteins propagation in aging and associated neurodegenerative disorders. *PLoS Computational Biology*, 10(11), e1003956. http://dx.doi.org/10.1371/journal.pcbi.1003956

Janke, A. L., De Zubicaray, G., Rose, S. E., Griffin, M., Chalk, J. B., & Galloway, G. J. (2001). 4D deformation modeling of cortical disease progression in Alzheimer's dementia. *Magnetic Resonance in Medicine*, 46, 661–666.

Kapur, S. (2003). Psychosis as a state of aberrant salience: A framework linking biology, phenomenology, and pharmacology in schizophrenia. *The American Journal of Psychiatry*, 160, 13–23.

Kohara, K., Kitamura, A., Morishima, M., & Tsumoto, T. (2001). Activity-dependent transfer of brain-derived neurotrophic factor to postsynaptic neurons. *Science (80-)*, 291, 2419–2423.

Kong, X.-Z., Mathias, S. R., Guadalupe, T., Glahn, D. C., Franke, B., Crivello, F., … Francks, C. (2018). Mapping cortical brain asymmetry in 17,141 healthy individuals worldwide via the ENIGMA Consortium. *Proceedings of the National Academy of Sciences*, 115, E5154–E5163. http://www.pnas.org/lookup/doi/10.1073/pnas.1718418115

Korth, C. (2012). Aggregated proteins in schizophrenia and other chronic mental diseases. *Prion*, 6, 134–141. http://www.tandfonline.com/doi/abs/10.4161/pri.18989

Laird, A. R., Eickhoff, S. B., Li, K., Robin, D. A., Glahn, D. C., & Fox, P. T. (2009). Investigating the functional heterogeneity of the default mode network using coordinate-based meta-analytic modeling. *The Journal of Neuroscience*, 29, 14496–14505. http://www.jneurosci.org/cgi/doi/10.1523/JNEUROSCI.4004-09.2009

Laird, A. R., Eickhoff, S. B., Rottschy, C., Bzdok, D., Ray, K. L., & Fox, P. T. (2013). Networks of task co-activations. *NeuroImage*, 80, 505–514. https://doi.org/10.1016/j.neuroimage.2013.04.073

Laird, A. R., Fox, P. M., Price, C. J., Glahn, D. C., Uecker, A. M., Lancaster, J. L., … Fox, P. T. (2005). ALE meta-analysis: Controlling the false discovery rate and performing statistical contrasts. *Human Brain Mapping*, 25, 155–164.

Laird, A. R., Lancaster, J. L., & Fox, P. T. (2005). BrainMap: The social evolution of a human brain mapping database. *Neuroinformatics*, 3, 65–78. http://link.springer.com/10.1385/NI:3:1:065

Lancaster, J. L., Tordesillas-Gutiérrez, D., Martinez, M., Salinas, F., Evans, A., Zilles, K., … Fox, P. T. (2007). Bias between MNI and Talairach coordinates analyzed using the ICBM-152 brain template. *Human Brain Mapping*, 28, 1194–1205. http://doi.wiley.com/10.1002/hbm.20345

Lancaster, J. L., Woldorff, M. G., Parsons, L. M., Liotti, M., Freitas, C. S., Rainey, L., … Fox, P. T. (2000). Automated Talairach Atlas labels for functional brain mapping. *Human Brain Mapping*, 10, 120–131.

Laughlin, S. B., & Sejnowski, T. J. (2003). Communication in neuronal networks. *Science (80-)*, 301, 1870–1874.

Leliveld, S. R., Bader, V., Hendriks, P., Prikulis, I., Sajnani, G., Requena, J. R., & Korth, C. (2008). Insolubility of disrupted-in-schizophrenia 1 disrupts oligomer-dependent interactions with nuclear distribution element 1 and is associated with sporadic mental disease. *The Journal of Neuroscience*, 28, 3839–3845. http://www.jneurosci.org/cgi/doi/10.1523/JNEUROSCI.5389-07.2008

Liao, X. H., Xia, M. R., Xu, T., Dai, Z. J., Cao, X. Y., Niu, H. J., … He, Y. (2013). Functional brain hubs and their test-retest reliability: A multiband resting-state functional MRI study. *NeuroImage*, 83, 969–982. https://doi.org/10.1016/j.neuroimage.2013.07.058

Liberati, A., Altman, D. G., Tetzlaff, J., Mulrow, C., Gotzsche, P. C., Ioannidis, J. P. A., … Moher, D. (2009). The PRISMA statement for reporting systematic reviews and meta-analyses of studies that evaluate healthcare interventions: explanation and elaboration. *BMJ*, 339, b2700–b2700. http://www.bmj.com/cgi/doi/10.1136/bmj.b2700

Liddle, E. B., Price, D., Palaniyappan, L., Brookes, M. J., Robson, S. E., Hall, E. L., … Liddle, P. F. (2016). Abnormal salience signaling in schizophrenia: The role of integrative beta oscillations. *Human Brain Mapping*, 37, 1361–1374. http://doi.wiley.com/10.1002/hbm.23107

Loewenstein, D. A., Barker, W. W., Chang, J. Y., Apicella, A., Yoshii, F., Kothari, P., … Duara, R. (1989). Predominant left hemisphere metabolic dysfunction in dementia. *Archives of Neurology*, 46, 146–152.

Mancuso, L., Costa, T., Nani, A., Manuello, J., Liloia, D., Gelmini, G., … Cauda, F. (2019). The homotopic connectivity of the functional brain: a meta-analytic approach. *Scientific Reports*, 9, 3346. https://doi.org/10.1038/s41598-019-40188-3

Mandelli, M. L., Vilaplana, E., Brown, J. A., Hubbard, H. I., Binney, R. J., Attygalle, S., … Gorno-Tempini, M. L. (2016). Healthy brain connectivity predicts atrophy progression in non-fluent variant of primary progressive aphasia. *Brain*, 139, 2778–2791.

Manoliu, A., Riedl, V., Zherdin, A., Mühlau, M., Schwerthöffer, D., Scherr, M., … Sorg, C. (2014). Aberrant dependence of default mode/central executive network interactions on anterior insular salience network activity in schizophrenia. *Schizophrenia Bulletin*, 40, 428–437.

Manuello, J., Nani, A., Premi, E., Borroni, B., Costa, T., Tatu, K., … Cauda, F. (2018). The pathoconnectivity profile of Alzheimer's disease: A morphometric coalteration network analysis. *Frontiers in Neurology*, 8, 1–15.

Margulies, D. S., Ghosh, S. S., Goulas, A., Falkiewicz, M., Huntenburg, J. M., Langs, G., … Smallwood, J. (2016). Situating the default-mode network along a principal gradient of macroscale cortical organization. *Proceedings of the National Academy of Sciences*, 113, 12574–12579. http://www.pnas.org/lookup/doi/10.1073/pnas.1608282113

Maslov, S., & Sneppen, K. (2002). Specificity and stability in topology of protein networks. *Science*, 296, 910–913. http://www.jstor.org.bibliopass.unito.it/stable/3076643

McTeague, L. M., Goodkind, M. S., & Etkin, A. (2016). Transdiagnostic impairment of cognitive control in mental illness. *Journal of Psychiatric Research*, 83, 37–46. https://doi.org/10.1016/j.jpsychires.2016.08.001

Mišić, B., Betzel, R. F., Nematzadeh, A., Goñi, J., Griffa, A., Hagmann, P., … Sporns, O. (2015). Cooperative and competitive spreading dynamics on the human connectome. *Neuron*, 86, 1518–1529.

Modinos, G., Vercammen, A., Mechelli, A., Knegtering, H., McGuire, P. K., & Aleman, A. (2009). Structural covariance in the hallucinating brain: A voxel-based morphometry study. *Journal of Psychiatry & Neuroscience*, 34, 465–469.

Moher, D., Liberati, A., Tetzlaff, J., & Altman, D. G. (2009). Preferred reporting items for systematic reviews and meta-analyses: The PRISMA statement. *Journal of Clinical Epidemiology*, 62, 1006–1012. http://linkinghub.elsevier.com/retrieve/pii/S0895435609001796

Navari, S., & Dazzan, P. (2009). Do antipsychotic drugs affect brain structure? A systematic and critical review of MRI findings. *Psychological Medicine*, 39, 1763–1777.

Neckelmann, G., Specht, K., Lund, A., Ersland, L., Smievoll, A. I., Neckelmann, D., & Hugdahl, K. (2006). MR morphometry analysis of grey matter volume reduction in schizophrenia: Association with hallucinations. *The International Journal of Neuroscience*, 116, 9–23.

Okada, N., Fukunaga, M., Yamashita, F., Koshiyama, D., Yamamori, H., Ohi, K., … Hashimoto, R. (2016). Abnormal asymmetries in subcortical brain volume in schizophrenia. *Molecular Psychiatry*, 21, 1460–1466. https://doi.org/10.1038/mp.2015.209

Palaniyappan, L. (2019). Inefficient neural system stabilization: A theory of spontaneous resolutions and recurrent relapses in psychosis. *Journal of Psychiatry & Neuroscience*, 44, 1–17.

Palaniyappan, L., & Liddle, P. F. (2012). Does the salience network play a cardinal role in psychosis? An emerging hypothesis of insular dysfunction. *Journal of Psychiatry & Neuroscience*, 37, 17–27.

Palaniyappan, L., White, T. P., & Liddle, P. F. (2013). The concept of salience network dysfunction in schizophrenia: From neuroimaging observations to therapeutic opportunities. *Current Topics in Medicinal*

Chemistry, 12, 2324–2338. http://www.eurekaselect.com/openurl/content.php?genre=article&issn=1568-0266&volume=12&issue=21&spage=2324

Pandya, S., Zeighami, Y., Freeze, B., Dadar, M., Collins, D. L., Dagher, A., & Raj, A. (2019). Predictive model of spread of Parkinson's pathology using network diffusion. NeuroImage, 192, 178–194. https://doi.org/10.1016/j.neuroimage.2019.03.001

Patel, R. S., Bowman, F. D., & Rilling, J. K. (2006). A Bayesian approach to determining connectivity of the human brain. Human Brain Mapping, 27, 267–276. http://doi.wiley.com/10.1002/hbm.20182

Perlson, E., Maday, S., M meng, F., Moughamian, A. J., & Holzbaur, E. L. F. (2010). Retrograde axonal transport: Pathways to cell death? Trends in Neurosciences, 33, 335–344. https://doi.org/10.1016/j.tins.2010.03.006

Pievani, M., de Haan, W., Wu, T., Seeley, W. W., & Frisoni, G. B. (2011). Functional network disruption in the degenerative dementias. Lancet Neurology, 10, 829–843. https://linkinghub.elsevier.com/retrieve/pii/S1474442211701582

Plaze, M., Bartrés-Faz, D., Martinot, J. L., Januel, D., Bellivier, F., De Beaurepaire, R., ... Paillère-Martinot, M. L. (2006). Left superior temporal gyrus activation during sentence perception negatively correlates with auditory hallucination severity in schizophrenia patients. Schizophrenia Research, 87, 109–115.

Raj, A., Kuceyeski, A., & Weiner, M. (2012). A network diffusion model of disease progression in dementia. Neuron, 73, 1204–1215. https://doi.org/10.1016/j.neuron.2011.12.040

Raj, A., & Powell, F. (2018). Models of network spread and network degeneration in brain disorders. Biological Psychiatry: Cognitive Neuroscience and Neuroimaging, 3, 788–797. https://doi.org/10.1016/j.bpsc.2018.07.012

Rubinov, M., & Sporns, O. (2010). Complex network measures of brain connectivity: Uses and interpretations. NeuroImage, 52, 1059–1069. https://doi.org/10.1016/j.neuroimage.2009.10.003

Salvador, R., Suckling, J., Coleman, M. R., Pickard, J. D., Menon, D., & Bullmore, E. (2005). Neurophysiological architecture of functional magnetic resonance images of human brain. Cerebral Cortex, 15, 1332–1342.

Saxena, S., & Caroni, P. (2011). Selective neuronal vulnerability in neurodegenerative diseases: From stressor thresholds to degeneration. Neuron, 71, 35–48. https://doi.org/10.1016/j.neuron.2011.06.031

Scarpazza, C., Tognin, S., Frisciata, S., Sartori, G., & Mechelli, A. (2015). False positive rates in voxel-based morphometry studies of the human brain: Should we be worried? Neuroscience and Biobehavioral Reviews, 52, 49–55. https://doi.org/10.1016/j.neubiorev.2015.02.008

Seeley, W. W., Crawford, R. K., Zhou, J., Miller, B. L., & Greicius, M. D. (2009). Neurodegenerative diseases target large-scale human brain networks. Neuron, 62, 42–52. https://doi.org/10.1016/j.neuron.2009.03.024

Sepulcre, J., Liu, H., Talukdar, T., Martincorena, I., Thomas Yeo, B. T., & Buckner, R. L. (2010). The organization of local and distant functional connectivity in the human brain. PLoS Computational Biology, 6, 1–15.

Shafiei, G., Markello, R. D., Makowski, C., Talpalaru, A., Kirschner, M., Devenyi, G. A., ... Mišić, B. (2019). Spatial patterning of tissue volume loss in schizophrenia reflects brain network architecture. Biological Psychiatry, 87, 727–735. https://linkinghub.elsevier.com/retrieve/pii/S0006322319317858

Sheline, Y. I., Barch, D. M., Price, J. L., Rundle, M. M., Vaishnavi, S. N., Snyder, A. Z., ... Raichle, M. E. (2009). The default mode network and self-referential processes in depression. Proceedings of the National Academy of Sciences, 106, 1942–1947. http://www.pnas.org/lookup/doi/10.1073/pnas.0812686106

Sporns, O., & Zwi, J. D. (2004). The small world of the cerebral cortex. Neuroinformatics, 2, 145–162. http://link.springer.com/10.1385/NI:2:2:145

Tatu, K., Costa, T., Nani, A., Diano, M., Quarta, D. G., Duca, S., ... Cauda, F. (2018). How do morphological alterations caused by chronic pain distribute across the brain? A meta-analytic co-alteration study.

NeuroImage: Clinical, 18, 15–30. https://doi.org/10.1016/j.nicl.2017.12.029

Thompson, P. M., Hayashi, K. M., de Zubicaray, G., Janke, A. L., Rose, S. E., Semple, J., ... Toga, A. W. (2003). Dynamics of gray matter loss in Alzheimer's disease. The Journal of Neuroscience, 23, 994–1005. http://www.jneurosci.org/lookup/doi/10.1523/JNEUROSCI.23-03-00994.2003

Thompson, P. M., Hayashi, K. M., Dutton, R. A., Chiang, M.-C., Leow, A. D., SowellL, E. R., ... Toga, A. W. (2007). Tracking Alzheimer's disease. Annals of the New York Academy of Sciences, 1097, 183–214. http://doi.wiley.com/10.1196/annals.1379.017

Thompson, P. M., Mega, M. S., Woods, R. P., Zoumalan, C. I., Lindshield, C. J., Blanton, R. E., ... Toga, A. W. (2001). Cortical change in Alzheimer's disease detected with a disease-specific population-based brain atlas. Cerebral Cortex, 11, 1–16. https://academic.oup.com/cercor/article-lookup/doi/10.1093/cercor/11.1.1

Torta, D. M. E., Costa, T., Duca, S., Fox, P. T., & Cauda, F. (2013). Parcellation of the cingulate cortex at rest and during tasks: A meta-analytic clustering and experimental study. Frontiers in Human Neuroscience, 7, 1–14. http://journal.frontiersin.org/article/10.3389/fnhum.2013.00275/abstract

Tropea, D., Hardingham, N., Millar, K., & Fox, K. (2018). Mechanisms underlying the role of DISC1 in synaptic plasticity. The Journal of Physiology, 596, 2747–2771.

Trossbach, S. V., Bader, V., Hecher, L., Pum, M. E., Masoud, S. T., Prikulis, I., ... Korth, C. (2016). Misassembly of full-length Disrupted-in-Schizophrenia 1 protein is linked to altered dopamine homeostasis and behavioral deficits. Molecular Psychiatry, 21, 1561–1572.

Turkeltaub, P. E., Eickhoff, S. B., Laird, A. R., Fox, M., Wiener, M., & Fox, P. (2012). Minimizing within-experiment and within-group effects in activation likelihood estimation meta-analyses. Human Brain Mapping, 33, 1–13.

Uddin, L. Q. (2015). Salience processing and insular cortical function and dysfunction. Nature Reviews Neuroscience, 16, 55–61. https://doi.org/10.1038/nrn3857

Van Essen, D. C., Smith, S. M., Barch, D. M., Behrens, T. E. J., Yacoub, E., & Ugurbil, K. (2013). The WU-Minn human connectome project: An overview. NeuroImage, 80, 62–79. https://doi.org/10.1016/j.neuroimage.2013.05.041

Vanasse, T. J., Fox, P. M., Barron, D. S., Robertson, M., Eickhoff, S. B., Lancaster, J. L., & Fox, P. T. (2018). BrainMap VBM: An environment for structural meta-analysis. Human Brain Mapping, 39, 3308–3325. http://doi.wiley.com/10.1002/hbm.24078

Warren, J. D., Rohrer, J. D., & Hardy, J. (2012). Disintegrating brain networks: From syndromes to molecular nexopathies. Neuron, 73, 1060–1062. https://doi.org/10.1016/j.neuron.2012.03.006

Warren, J. D., Rohrer, J. D., Schott, J. M., Fox, N. C., Hardy, J., & Rossor, M. N. (2013). Molecular nexopathies: A new paradigm of neurodegenerative disease. Trends in Neurosciences, 36, 561–569. https://linkinghub.elsevier.com/retrieve/pii/S0166223613001288

Watts, D. J., Strogatz, S. H., & Tseng, Y.-M. (1998). Collective dynamics of 'small-world' networks. Nature, 153, 810–817. https://doi.org/10.1049/ip-com:20050366%5Cnhttp://search.ebscohost.com/login.aspx?direct=true&db=bth&AN=23157160&site=bsi-live&scope=site

Wheeler, A. L., Felsky, D., Viviano, J. D., Stojanovski, S., Ameis, S. H., Szatmari, P., ... Voineskos, A. N. (2017). BDNF-dependent effects on amygdala–cortical circuitry and depression risk in children and youth. Cerebral Cortex, 28, 1760–1770.

Wheeler, A. L., Wessa, M., Szeszko, P. R., Foussias, G., Chakravarty, M. M., Lerch, J. P., ... Voineskos, A. N. (2015). Further neuroimaging evidence for the deficit subtype of schizophrenia: A cortical connectomics analysis. JAMA Psychiatry, 72, 446–455.

White, T. P., Joseph, V., Francis, S. T., & Liddle, P. F. (2010). Aberrant salience network (bilateral insula and anterior cingulate cortex) connectivity during information processing in schizophrenia. Schizophrenia Research, 123, 105–115. https://doi.org/10.1016/j.schres.2010.07.020

World Health Organisation. (1992). *The ICD-10 classification of mental and behavioural disorders: Clinical descriptions and diagnostic guidelines*. Geneva: WHO. https://apps.who.int/iris/handle/10665/37108

Yeh, F. C., Badre, D., & Verstynen, T. (2016). Connectometry: A statistical approach harnessing the analytical potential of the local connectome. *NeuroImage*, *125*, 162–171. https://doi.org/10.1016/j.neuroimage.2015.10.053

Yeh, F. C., Liu, L., Hitchens, T. K., & Wu, Y. L. (2017). Mapping immune cell infiltration using restricted diffusion MRI. *Magnetic Resonance in Medicine*, *77*, 603–612.

Yeh, F.-C., Panesar, S., Fernandes, D., Meola, A., Yoshino, M., Fernandez-Miranda, J. C., ... Verstynen, T. (2018). Population-averaged atlas of the macroscale human structural connectome and its network topology. *NeuroImage*, *178*, 57–68. https://linkinghub.elsevier.com/retrieve/pii/S1053811918304324

Yeh, F. C., Verstynen, T. D., Wang, Y., Fernández-Miranda, J. C., & Tseng, W. Y. I. (2013). Deterministic diffusion fiber tracking improved by quantitative anisotropy. *PLoS One*, *8*, 1–16.

Zhou, J., Gennatas, E. D., Kramer, J. H., Miller, B. L., & Seeley, W. W. (2012). Predicting regional neurodegeneration from the healthy brain functional connectome. *Neuron*, *73*, 1216–1227. http://linkinghub.elsevier.com/retrieve/pii/S0896627312002279

Zhu, S., Abounit, S., Korth, C., & Zurzolo, C. (2017). Transfer of disrupted-in-schizophrenia 1 aggregates between neuronal-like cells occurs in tunnelling nanotubes and is promoted by dopamine. *Open Biology*, *7*(3), 160328. http://dx.doi.org/10.1098/rsob.160328

SUPPORTING INFORMATION

Additional supporting information may be found online in the Supporting Information section at the end of this article.